

https://dspace.org/

Quantum skyrmions in general quantum channels

Robert De Mello Koch; Bo-Qiang Lu; Pedro Ornelas; Isaac Nape; Andrew Forbes

https://hdl.handle.net/10539/46015
DOAJ

Downloaded from a DSpace repository. https://dspace.org/

APL Quantum

RESEARCH ARTICLE | MAY 19 2025

Quantum skyrmions in general quantum channels

Robert de Mello Koch ; Bo-Qiang Lu ; Pedro Ornelas ; Isaac Nape ; Andrew Forbes

Check for updates

APL Quantum 2, 026126 (2025)
https://doi.org/10.1063/5.0271868

View Online
Export Citation

Articles You May Be Interested In

Oscillations of the total kinematic momentum vector for viscous fluid dynamics in pipes of arbitrary section

Physics of Fluids (August 2023)

19 May 2025 14:12:42



APL Quantum
Special Topics
Open for Submissions

Submit Today!

AIP Publishing

AIP Publishing

Quantum skyrmions in general quantum channels

Cite as: APL Quantum 2, 026126 (2025); doi: 10.1063/5.0271868
Submitted: 20 March 2025 • Accepted: 30 April 2025 •
Published Online: 19 May 2025

View Online Export Citation CrossMark

Robert de Mello Koch,[1,2,a] Bo-Qiang Lu,[1] Pedro Ornelas,[3] Isaac Nape,[3] and Andrew Forbes[3,a]

AFFILIATIONS

[1] School of Science, Huzhou University, Huzhou 313000, China
[2] Mandelstam Institute for Theoretical Physics, School of Physics, University of the Witwatersrand, Private Bag 3, Wits 2050, South Africa
[3] School of Physics, University of the Witwatersrand, Private Bag 3, Wits 2050, South Africa

[a] **Authors to whom correspondence should be addressed:** robert.demellokoch@gmail.com and andrew.forbes@wits.ac.za

ABSTRACT

Quantum skyrmions as topologically structured entangled states have the potential to be a pathway toward robustness against external perturbations, but so far no theoretical framework exists to validate this. Here, we introduce the notion of a new entanglement observable based on such topologies and develop a theoretical framework for studying its evolution in general quantum channels. Using photons entangled in orbital angular momentum and polarization as an example, we show that the noise affecting both photons can be recast as a position-dependent perturbation affecting only the photon in the polarization state, restricting the noise to a finite-dimensional Hilbert space. From this we predict complete resilience for both non-depolarizing and depolarizing noise, the former by rigorous arguments based on homotopic maps and the latter by numerical simulation. Finally, we identify sources of local noise that can destabilize the topology and suggest why this may be ignored in practical situations. Our work sets a solid foundational framework for understanding how and why topology enhances the resilience of such entanglement observables, with immediate relevance to the distribution of information through entanglement in noisy environments, such as quantum computers and quantum networks.

© 2025 Author(s). All article content, except where otherwise noted, is licensed under a Creative Commons Attribution (CC BY) license (https://creativecommons.org/licenses/by/4.0/). https://doi.org/10.1063/5.0271868

19 May 2025 14:12:42

I. INTRODUCTION

Entanglement is a key enabler for a wide range of quantum technologies, including quantum key distribution,[1–3] quantum secret sharing,[4,5] quantum superdense coding,[6,7] and quantum computing,[8,9] promising enhanced secure communication networks and computing platforms. Its functionality can be enhanced by tailoring the correlations using various degrees of freedom of photons beyond just polarization, for instance orbital angular momentum (OAM)[10,11] and temporal/wavelength,[12–14] and by mixing them to produce hybrid[15–18] and hyper[19–22] entangled states. However, entanglement is fragile and decays rapidly when subjected to decoherence and dephasing channels, resulting in actions such as a change of basis, phase errors, or evolution from pure and entangled to noisy and mixed states.[23–25]

An exciting prospect is the use of topologies[26] to preserve entanglement, often enabled by topological matter.[27–31] Recently the notion of optical topologies has emerged in the form of skyrmions,[32,33] with exciting opportunities for using structured matter for topology creation[34,35] as well as exchanging topology between light and matter.[36,37] One manifestation of optical skyrmions is as tailored quantum photonic wave functions,[38] with the prospect of preserving quantum information encoded in topology. However, unlike its magnetic counterpart, there is no natural interaction mechanism or energy barrier to photonic topology, so the question of its resilience remains open.[39] As yet, classical topology through complex channels has returned some positive[40] and some negative[41] results, while in the quantum case only a unitary amplitude-damping channel[38] and isotropic noise have been considered.[42] It remains unknown whether quantum topology is preserved in the presence of general quantum channels, essential if it is to be utilized for quantum information processing and communication.

Here, we outline a foundational theoretical treatment for quantum topologies in quantum channels. In particular, we answer the

© Author(s) 2025

question of the robustness of quantum skyrmions, predicting which channels they are resilient to while unveiling the intricacies and nuances of dealing with maps to which the states are not robust. For non-depolarizing sources of noise, our description employs a quantum channel with a single Kraus operator, allowing for a rigorous argument based on homotopies between the noisy and noise-free density matrices, substantiating the topological noise rejection property. For decoherence channels where the operators are convex sums of Kraus operators, we show that although noise rejection is not simply established using homotopies, transitions between distinct topological numbers are not easily induced by noise, thereby enabling our scheme to benefit from a topological encoding of the entangled states. Our framework will be essential in the understanding and deployment of topology as a mechanism for resilience of quantum information in noisy environments, such as quantum computers and quantum networks.

II. THE SKYRMION WAVE FUNCTION

The skyrmion wave function is a pure state of two entangled photons. The first, photon A, occupies an orbital angular momentum state in a Hilbert space $\mathcal{H}_A$. The second, photon B, is in a polarization state in a Hilbert space $\mathcal{H}_B$. The two photon state belongs to the tensor product $\mathcal{H}_A \otimes \mathcal{H}_B$. A typical skyrmion wave function takes the form

$$|\psi\rangle = \int |\vec{r}_A\rangle \left(u_0^{l_1}(\vec{r}_A)|H\rangle_B + u_0^{l_2}(\vec{r}_A)e^{i\alpha}|V\rangle_B \right) d^3 r_A, \tag{1}$$

where α is an arbitrary phase, l_1 and l_2 are orbital angular momentum quantum numbers, and the Laguerre–Gaussian modes are

$$u_0^l(\rho,\phi) = \sqrt{\frac{2}{\pi |l|!}} \frac{1}{w_0} \left(\frac{\sqrt{2}\rho}{w_0} \right)^{|l|} \exp\left(-\frac{\rho^2}{w_0^2} \right) L_0^{|l|}\left(\frac{2\rho^2}{w_0^2} \right) \exp(il\phi), \tag{2}$$

where L is the generalized Laguerre polynomial and w_0 is the Gaussian width. This state is described by the density matrix $\hat{\rho} = |\psi\rangle\langle\psi|$.[43] In terms of this density matrix, the Stokes parameters are

$$S_j(\vec{r}_A) = \mathrm{Tr}_B\left(\langle \vec{r}_A|\hat{\rho}|\vec{r}_A\rangle \, \sigma_{Bj} \right) \qquad j = x, y, z, \tag{3}$$

where σ_{Bj} is a Pauli matrix σ_j acting on $\mathcal{H}_B$,

$$\sigma_x = \begin{pmatrix} 0 & 1 \\ 1 & 0 \end{pmatrix} \quad \sigma_y = \begin{pmatrix} 0 & -i \\ i & 0 \end{pmatrix} \quad \sigma_z = \begin{pmatrix} 1 & 0 \\ 0 & -1 \end{pmatrix}. \tag{4}$$

Normalize the Stokes parameters to define a unit vector $(\tilde{S}_i)$ that describes a point on a two sphere S^2 at each $\vec{r}_A$,

$$\tilde{S}_j = \alpha S_j \qquad j = x, y, z \qquad \sum_j \tilde{S}_j \tilde{S}_j = 1, \tag{5}$$

where α is fixed by the normalization condition $\vec{\tilde{S}} \cdot \vec{\tilde{S}} = 1$.

The map $\tilde{S}_j(x,y)$ plays a central role. Its base space is the set of all points on a two dimensional plane, which itself maps to a two sphere after compactifying and employing a stereographic map. Since $\tilde{S}_j(x,y)$ is a normalized vector, the target space of this map is also a two sphere—the Poincaré sphere. Consequently, $\tilde{S}_j(x,y)$ maps a two sphere to a two sphere. Any map of this type has an associated winding number, which counts how many times the first two spheres are wrapped around the second. In this context, the winding number is called the skyrmion number, and it may be computed as

$$N = \frac{1}{4\pi} \int_{-\infty}^{\infty} \int_{-\infty}^{\infty} \Sigma_z(x,y) \, dx \, dy,$$
$$\Sigma_z(x,y) = \epsilon_{pqr} \tilde{S}_p \frac{\partial \tilde{S}_q}{\partial x} \frac{\partial \tilde{S}_r}{\partial y}. \tag{6}$$

For the wave function given earlier, we can easily verify that

$$N = l_1 - l_2. \tag{7}$$

A product wave function, which is, therefore, not entangled, would map all points in the base space to a single point on the Poincaré sphere. This is a map with winding number zero. A non-zero winding number indicates that the map cannot be reduced to a trivial (constant) map without tearing or discontinuity. Therefore, the map wraps around the target space in a non-trivial way, which cannot be undone by any smooth deformation. This non-trivial wrapping is simultaneously a manifestation of non-trivial topology and the fact that the wave function is not a product, i.e., that it is entangled. This observation reveals a profound connection between topology and entanglement, and it is the winding number N that provides the discretization of entanglement. The key question we address in this study is how noise affects the value of N.

III. NOISE MODEL

In this section, we aim to introduce a noise model that is comprehensive enough to accurately reflect real-world physical systems. To begin, we might consider a scenario where photons A and B are analyzed separately, as depicted in Fig. 1(a). This approach involves understanding how the states of photons A and B transform under various types of spatial and polarization noise, respectively. Given the complexity of the infinite-dimensional Hilbert space for photon A, this task can be daunting. Instead, by leveraging the explicit form of the skyrmion wave function (1), we simplify our analysis.[44] This approach confines the effect of noise to the polarization state of photon B, streamlining the problem. To ensure that our description remains comprehensive, we must allow for position-dependent noise, as illustrated in Fig. 1(b). Our model captures the impact of noise on the density matrix, and accounting for its effect on the skyrmion number is then a straightforward extension using formulas (3), (5), and (6). In our analysis, we model realistic environmental noise acting on OAM and polarization photons as position-dependent polarization noise. To avoid confusion, we emphasize that this differs from the conventional notion of noise, which typically refers to the environment's tendency to convert pure states into mixed states.

Noise can, in general, affect the states of both photons in the entangled skyrmion state (1). To account for this, consider noise induced perturbations of the form[45]

$$u_0^{l_i}(\vec{r}_A) \to u_0^{l_i}(\vec{r}_A) + u_{\mathrm{pert}}^{l_i}(\vec{r}_A) \qquad i = 1, 2,$$
$$|P\rangle_B \to |P\rangle_B + |P_{\mathrm{pert}}\rangle_B \qquad P = H, V. \tag{8}$$

19 May 2025 14:12:42

© Author(s) 2025

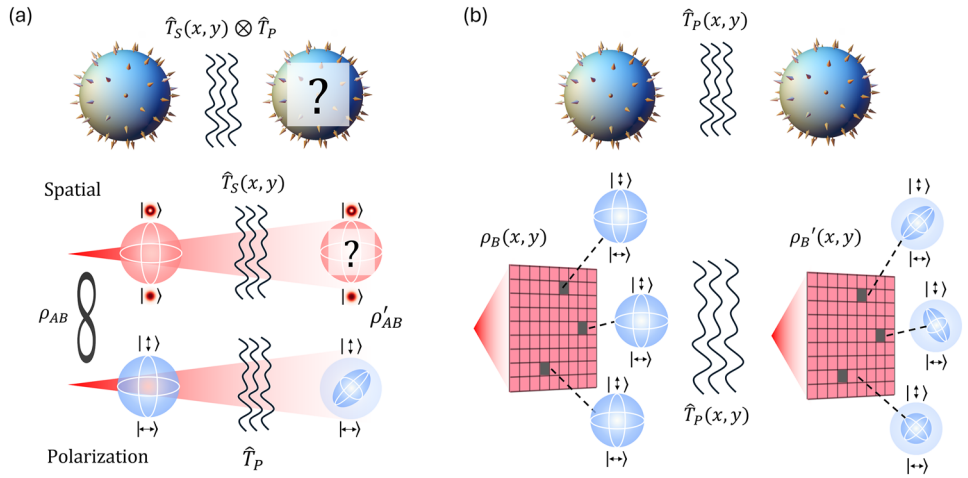


FIG. 1. Skyrmion noise model. Photons A and B are entangled in space and polarization, respectively, such that their entanglement exhibits non-trivial topological features. (a) Investigating the general behavior of such features under the influence of noise requires passing photon A (spatial) through a noise channel ($\hat{T}_S(x,y)$), which modulates the amplitude and phase of the photon at different points in space, and photon B (polarization) through a channel ($\hat{T}_P$), which transforms its polarization. (b) By exploiting the explicit form of the skyrmion wave function, a more convenient model can be used that considers the noise as only influencing the polarization of photon B at different points in space ($\hat{T}_P(x,y)$), i.e., a position-dependent source of noise acting only on the polarization degree of freedom.

Our notation is to denote the change in a quantity due to a perturbation with a subscript "pert." In the above-mentioned formula, $u^{l_i}_{\text{pert}}(\vec{r}_A)$ is the change in $u^{l_i}_0(\vec{r}_A)$ due to the perturbation, and $|P_{\text{pert}}\rangle_B$ is the change in $|P\rangle_B$ due to the perturbation. These changes due to the perturbation are not all independent since the trace of the density matrix must always be preserved. This gives a constraint written as an equation for the integral over the fluctuations. Since it is not very constraining or illuminating, we do not explore it further. The most practical way to proceed is simply to ignore the constraint and then normalize the trace of the noisy density matrix to 1 before it is interpreted. By adding the noise perturbations, we obtain the following noisy state:

$$|\psi\rangle_{\text{noisy}} = \int |\vec{r}_A\rangle \Big(u^{l_1}_0(\vec{r}_A)(|H\rangle_B + |H_{\text{pert}}\rangle_B) + u^{l_2}_0(\vec{r}_A)e^{i\alpha}(|V\rangle_B + |V_{\text{pert}}\rangle_B) \Big) d^3 r_A, \tag{9}$$

where

$$|H_{\text{pert}}\rangle_B = \frac{u^{l_1}_{\text{pert}}(\vec{r}_A)}{u^{l_1}_0(\vec{r}_A)}|H\rangle_B + |H_{\text{pert}}\rangle_B + \frac{u^{l_1}_{\text{pert}}(\vec{r}_A)}{u^{l_1}_0(\vec{r}_A)}|H_{\text{pert}}\rangle_B,$$
$$|V_{\text{pert}}\rangle_B = \frac{u^{l_2}_{\text{pert}}(\vec{r}_A)}{u^{l_2}_0(\vec{r}_A)}|V\rangle_B + |V_{\text{pert}}\rangle_B + \frac{u^{l_2}_{\text{pert}}(\vec{r}_A)}{u^{l_2}_0(\vec{r}_A)}|V_{\text{pert}}\rangle_B.$$

We have manipulated the noisy state (9) so that it looks as if photon A is completely unaffected by noise. The price for this is that the polarization vectors of photon B suffer position dependent noise. This manipulation relies heavily on the detailed form of the skyrmion wave function (1). This is not a loss of generality, since the skyrmion number itself is tied to this state. The clear advantage of this point of view is that we are now adding noise to the finite dimensional Hilbert space of polarization states of photon B. This immediately allows us to profitably employ both the language and ideas developed to study noisy qubits, as well as recent advances in quantum polarimetry. Note that if the OAM space is treated as two-dimensional, then *many* such subspaces would exist, all potentially giving rise to their own topological numbers, i.e., the measurement choice itself will affect the outcome. The entanglement itself could appear to decrease if only a reduced space is used, even for unitary channels. Specifically, the fact that we add noise to a finite dimensional Hilbert space allows us to phrase the discussion in terms of noise channels, using the notion of a quantum operation $\mathcal{E}$, which maps density matrices to density matrices. The operator sum representation of $\mathcal{E}$ is

$$\mathcal{E}(\hat{\rho}) = \sum_i E_i \hat{\rho} E_i^\dagger \qquad \sum_i E_i^\dagger E_i = \mathbf{1}, \tag{10}$$

where the E_i are known as Kraus operators. Quantum polarimetry will determine the structure of the Kraus operators. For further references dealing with open quantum systems in general and with the Kraus theorem, see Refs. 46–49.

It is important to clarify certain aspects of our noise model to pre-empt potential misconceptions. In our earlier discussion, we introduced position-dependent polarization noise. However, it would be incorrect to conflate this with standard polarization noise. Our reformulation was not intended to directly model specific physical noise sources, but rather to ensure that all such sources are collectively described by a position-dependent completely positive

19 May 2025 14:12:42

© Author(s) 2025

trace-preserving (CPTP) map. This provides the most general transformation applicable to the density matrix of photon B, enabling a universal framework for describing perturbations to the system. Therefore, this framework makes no explicit assumptions about any particular noise channel configuration, thereby rendering it applicable to any real-world scenario where photons may propagate through noisy quantum channels in a variety of different ways.

In the special case where perturbations exhibit no position dependence, they can be interpreted as affecting only photon B. Likewise, if the perturbations do not mix the polarization states $|V\rangle$ and $|H\rangle$ and affect both identically, they correspond to a perturbation of photon A. More generally, when the model yields a perturbation that is both position-dependent and acts differently on the two polarization states, both photons undergo a non-trivial transformation.

Finally, we previously stated that our model is rewritten in a form where photon A appears to be completely unaffected by the noise. A natural objection to this claim is that tracing over photon B results in a reduced density matrix for photon A that is undeniably altered. How, then, can we assert that photon A remains unaffected?

The key point is that whenever we have an entangled state of two particles, any operation acting solely on one particle—and subsequently tracing it out—will inevitably influence the reduced density matrix of the other particle. This fundamental property of entanglement is precisely what we leverage in constructing our noise model.

IV. QUANTUM THEORY OF POLARIMETRY

In this section, we review relevant aspects of the framework of polarimetry in terms of quantum mechanical operators acting on quantum states of light, as developed in Ref. 50. Polarization is characterized by four Stokes parameters, and polarimetry involves the 4×4 Mueller matrix, which governs the linear transformations of these parameters under various optical elements. The approach in Ref. 50 extends this to the quantum domain by describing quantum channels that correspond to Mueller matrices. For the quantum Stokes operators to align with the predictions of classical polarimetry, they must transform according to Mueller calculus, irrespective of the quantum state. A few basic quantum operations form the building blocks of quantum polarimetry. These building blocks are combined into composite quantum operations to realize the degrees of freedom of an arbitrary Mueller matrix. One significant implication of the quantum channels described here is that polarimetry can consistently be represented in a trace-preserving manner. This ensures total probability conservation for both deterministic and non-deterministic Mueller matrices, even though some information may leak to the environment about the states and transformations involved.

A. Stokes operators

The electric field of a monochromatic electromagnetic wave propagating along the $\vec{k}$ direction is given by

$$\vec{E}(\vec{r},t) = (h\vec{h} + v\vec{v})e^{i\vec{k}\cdot\vec{r}-i\omega t}, \tag{11}$$

where h, v are two complex constants and $\vec{h}, \vec{v}$ are two vectors orthogonal to the direction of propagation $\vec{k}$. The polarization properties of the field $\vec{E}$ are characterized by the Stokes parameters

$$\begin{aligned} S_0 &= |h|^2 + |v|^2, \qquad S_1 = |h|^2 - |v|^2, \\ S_2 &= h^* v + v^* h, \qquad S_3 = -i(h^* v - v^* h), \end{aligned} \tag{12}$$

as usual. Only three of these parameters are independent, since

$$S_0^2 = S_1^2 + S_2^2 + S_3^2. \tag{13}$$

The Stokes vector

$$\vec{S} = (S_1, S_2, S_3), \tag{14}$$

after normalizing by S_0, spans the Poincaré sphere. For the description of stochastic light, the Stokes parameters are given as time or ensemble averages. Consequently, $\vec{S}/S_0$ typically lies inside the Poincaré sphere. This motivates the definition of the degree of polarization

$$p = \frac{|\vec{S}|}{S_0}. \tag{15}$$

To develop a quantum mechanical description, it is cleanest to consider the field in some finite volume, which renders the modes of the field discrete. Toward this end, imagine the electric field is contained inside a cavity (or region) of volume V. The field $\vec{E}$ is quantized by promoting h and v to operators as follows:[51]

$$h \to \sqrt{\frac{\hbar\omega}{2V\epsilon_0}}\hat{a}_H^\dagger, \qquad v \to \sqrt{\frac{\hbar\omega}{2V\epsilon_0}}\hat{a}_V^\dagger. \tag{16}$$

These are the usual bosonic oscillators, which obey the Fock space algebra

$$[\hat{a}_i, \hat{a}_j^\dagger] = \delta_{ij} \qquad [\hat{a}_i^\dagger, \hat{a}_j^\dagger] = 0 = [\hat{a}_i, \hat{a}_j]. \tag{17}$$

Following[50] transform to a circularly polarized basis

$$\hat{a}_L = \frac{\hat{a}_H - i\hat{a}_V}{\sqrt{2}}, \qquad \hat{a}_R = \frac{\hat{a}_H + i\hat{a}_V}{\sqrt{2}}. \tag{18}$$

In terms of these oscillators, we can define the Stokes operators as follows:

$$\begin{aligned} \hat{S}_0 &= \hat{a}_L^\dagger\hat{a}_L + \hat{a}_R^\dagger\hat{a}_R, \qquad \hat{S}_1 = \hat{a}_L^\dagger\hat{a}_R + \hat{a}_R^\dagger\hat{a}_L, \\ \hat{S}_2 &= -i(\hat{a}_L^\dagger\hat{a}_R - \hat{a}_R^\dagger\hat{a}_L), \qquad \hat{S}_3 = \hat{a}_L^\dagger\hat{a}_L - \hat{a}_R^\dagger\hat{a}_R. \end{aligned} \tag{19}$$

The classical Stokes parameters are recovered as expectation values of these operators. It is not possible to do better: since the Stokes operators do not commute, simultaneous eigenvectors with eigenvalues given by the classical values of the Stokes parameters simply do not exist. The Stokes operators obey the u(2) algebra

$$[\hat{S}_\mu, \hat{S}_\nu] = 2i(1-\delta_{\mu 0})(1-\delta_{\nu 0})\sum_{j=1}^{3}\epsilon_{\mu\nu j}\hat{S}_j, \tag{20}$$

and respect the constraint

$$\hat{S}_1^2 + \hat{S}_2^2 + \hat{S}_3^2 = \hat{S}_0^2 + 2\hat{S}_0, \tag{21}$$

19 May 2025 14:12:42

© Author(s) 2025

which is the quantum analog of (13). The reason why we obtain $u(2)$ and not $su(2)$ is that $\hat{S}_0$ is an extra generator commuting with $\hat{S}_1$, $\hat{S}_2$, and $\hat{S}_3$. It is interesting to note that since we are forced to use expectation values to connect to the classical description, there are many distinct quantum states that lead to the same set of classical Stokes parameters.

B. Mueller matrices, Jones matrices, and quantum channels

It is an empirical fact that different materials linearly transform the polarization properties of the incident light. The four Stokes parameters change as follows:

$$S_\mu \to S'_\mu = \sum_{\nu=0}^{3} M_{\mu\nu} S_\nu, \tag{22}$$

where the 4×4 matrix $M_{\mu\nu}$ is known as the Mueller matrix. Mueller matrices are broadly categorized as either depolarizing or non-depolarizing. Non-depolarizing Mueller matrices can be described using Jones matrices J, which represent an $\mathrm{SL}(2,\mathbb{C})$[52] transformation on the electric field,

$$|E\rangle \equiv \begin{bmatrix} h \\ v \end{bmatrix} \to \begin{bmatrix} J_{11} & J_{12} \\ J_{21} & J_{22} \end{bmatrix} \begin{bmatrix} h \\ v \end{bmatrix} \equiv J|E\rangle. \tag{23}$$

The non-depolarizing Mueller matrices do not change the degree of polarization of perfectly polarized incident light. The depolarizing Mueller matrices are described as ensemble averages of Jones matrices

$$|E\rangle\langle E| \to \sum_i \lambda_i J_i |E\rangle\langle E| J_i^\dagger, \tag{24}$$

and they reduce the degree of polarization of perfectly polarized incident light. Partially polarized light can have its degree of polarization both increase and decrease under the effect of both depolarizing and non-depolarizing optical systems. Non-depolarizing systems are also called deterministic since they are realized as pure Jones matrices, while depolarizing systems are non-deterministic because they are realized as ensemble averages of Jones matrices. This language has a natural parallel for quantum systems.

It is straightforward to derive a relationship between the Jones matrices and the Mueller matrices. In terms of the Pauli matrices (4) and the 2×2 identity matrix σ_0, it is simple to verify that[53]

$$|E\rangle\langle E| = \frac{1}{2}(\sigma_0 S_0 + \sigma_1 S_2 + \sigma_2 S_3 + \sigma_3 S_1) = \frac{1}{2}\sum_{\mu=0}^{3}\sum_{\nu=0}^{3} \sigma_\mu A_{\mu\nu} S_\nu, \tag{25}$$

with

$$A = \begin{bmatrix} 1 & 0 & 0 & 0 \\ 0 & 0 & 1 & 0 \\ 0 & 0 & 0 & 1 \\ 0 & 1 & 0 & 0 \end{bmatrix}. \tag{26}$$

This implies that

$$S_\mu = \sum_{\nu=0}^{3} A^T_{\mu\nu} \mathrm{Tr}\,(\sigma_\nu |E\rangle\langle E|), \tag{27}$$

where A^T is the usual matrix transpose of A. Under the action of the Jones matrix, we have

$$\begin{aligned} S_\mu \to S'_\mu &= \sum_{\nu=0}^{3} A^T_{\mu\nu} \mathrm{Tr}\,(\sigma_\nu J|E\rangle\langle E|J^\dagger) \\ &= \frac{1}{2}\sum_{\nu=0}^{3}\sum_{\alpha=0}^{3}\sum_{\beta=0}^{3} A^T_{\mu\nu} \mathrm{Tr}\,(\sigma_\nu J \sigma_\alpha J^\dagger) A_{\alpha\beta} S_\beta \\ &= \sum_{\beta=0}^{3} M_{\mu\beta} S_\beta. \end{aligned} \tag{28}$$

From this, we can read off the relation between the Mueller matrix and the Jones matrix (for a relevant and related textbook discussion, see Sec. 8.3.2 of Ref. 46),

$$M_{\mu\beta} = \frac{1}{2}\sum_{\nu=0}^{3}\sum_{\alpha=0}^{3} A^T_{\mu\nu} \mathrm{Tr}\,(\sigma_\nu J \sigma_\alpha J^\dagger) A_{\alpha\beta}. \tag{29}$$

The density matrix for photon B will appear exactly as $|E\rangle\langle E|$ appears in the above-mentioned discussion. This makes it clear that the Jones matrices are the Kraus operators of the operator sum representation for the noise channel. The discussion of the Kraus operators acting on the density matrix of the state can be phrased, after using (28), in terms of an affine mapping of the Stokes vectors.

Mueller matrices for common elements used to control polarization are well known, and we will use these descriptions to construct noise models. These elements include the following steps:

1. **Retarders:** Maintain the intensity S_0 and the degree of polarization p, but they rotate the polarization vector $\vec{S}$ so that they are deterministic. The Mueller matrix is
$$M_R = \begin{bmatrix} 1 & 0 \\ 0^T & R \end{bmatrix}, \tag{30}$$
where R is a 3×3 rotation matrix.
2. **Diattenuators:** Differentially transmit light incident with different polarization directions. They take perfectly polarized light to perfectly polarized light at a reduced intensity so that they are also deterministic. The Mueller matrix is $(0 < q, r < 1)$
$$M_D = \begin{bmatrix} \frac{q+r}{2} & \frac{q-r}{2} & 0 & 0 \\ \frac{q-r}{2} & \frac{q+r}{2} & 0 & 0 \\ 0 & 0 & \sqrt{qr} & 0 \\ 0 & 0 & 0 & \sqrt{qr} \end{bmatrix}. \tag{31}$$
Setting $r = 0$ and $q = 1$ in M_D gives a Mueller matrix for the linear polarizer.
3. **Depolarizers:** Maintain the total intensity S_0 but reduce the degree of polarization p of perfectly polarized light. The Mueller matrix is
$$M_d = \begin{bmatrix} 1 & 0 \\ 0^T & m \end{bmatrix}, \tag{32}$$
where m is a 3×3 symmetric matrix with eigenvalues between -1 and 1.

19 May 2025 14:12:42

© Author(s) 2025

4. **Arbitrary Mueller Matrices:** Can be decomposed into the sequential application of a diattenuator, a retarder, and a depolarizer $M = M_d M_D M_R$.

It is possible to derive the quantum operation that corresponds to any given Mueller matrix. General quantum channels are represented by completely positive and trace preserving (CPTP) maps acting on the density matrix $\hat{\rho} = |E\rangle\langle E|$,

$$\mathcal{E}(\hat{\rho}) = \sum_l \hat{K}_l \hat{\rho} \hat{K}_l^\dagger \qquad \sum_l \hat{K}_l^\dagger \hat{K}_l = \mathbf{1}. \tag{33}$$

This is called the operator sum representation of the channel, and the operators $\hat{K}_l$ are known as Kraus operators. Composite quantum channels are produced as products or sums of other quantum channels. The application of Mueller matrix M_1 followed by M_2 constructs the composite channel

$$\mathcal{E}_{M_2 M_1}(\hat{\rho}) = \mathcal{E}_{M_2}(\mathcal{E}_{M_1}(\hat{\rho})), \tag{34}$$

while a linear combination of matrices M_1 and M_2 constructs the channel

$$\mathcal{E}_{p_1 M_1 + p_2 M_2}(\hat{\rho}) = p_1\ \mathcal{E}_{M_1}(\hat{\rho}) + p_2\ \mathcal{E}_{M_2}(\hat{\rho}). \tag{35}$$

Synthesizing more complicated quantum channels from simpler building blocks reduces the problem of constructing the channel for an arbitrary Mueller matrix to that of constructing channels for retarders, diattentuators, and depolarizers. This construction is straightforward, as we now explain.

1. Quantum channels for retarders

To realize the retarder, (30) instructs us to construct a rotation. The Mueller matrix in (30) acts on the Stokes parameters S_1, S_2, and S_3. We need to construct a Jones matrix, which will act on the state of our polarization photon (photon B). The relevant argument is given in (28). Concretely [$i, j = 1, 2, 3$ and A_{ij} is the lower right 3×3 block of matrix A defined in (26)]

$$\begin{aligned} S_i &= \sum_{j=1}^{3} A_{ij}^T \mathrm{Tr}\left(\sigma_j J|E\rangle\langle E|J^\dagger\right) \\ &= \frac{1}{2}\sum_{j=1}^{3}\sum_{k=1}^{3}\sum_{l=1}^{3} A_{ij}^T \mathrm{Tr}\left(\sigma_j J \sigma_k J^\dagger\right) A_{kl} S_l \\ &= \sum_{l=1}^{3} R_{ik} S_l, \end{aligned} \tag{36}$$

so that we read off[54]

$$R_{ik} = \frac{1}{2}\sum_{j=1}^{3}\sum_{k=1}^{3}\sum_{l=1}^{3} A_{ij}^T \mathrm{Tr}\left(\sigma_j J \sigma_k J^\dagger\right) A_{kl}. \tag{37}$$

This relation can be used to verify that the rotation is represented using Euler angles

$$R^T = \begin{bmatrix} \cos\theta\cos\varphi\cos\psi - \sin\varphi\sin\psi & \cos\psi\sin\varphi + \cos\theta\cos\varphi\sin\psi & -\cos\varphi\sin\theta \\ -\cos\theta\cos\psi\sin\varphi - \cos\varphi\sin\psi & \cos\psi\cos\varphi - \cos\theta\sin\varphi\sin\psi & \sin\varphi\sin\theta \\ \cos\psi\sin\theta & \sin\theta\sin\psi & \cos\theta \end{bmatrix}, \tag{38}$$

corresponds to the Jones matrix[55]

$$J_R(\theta, \varphi, \psi) = \begin{bmatrix} e^{-\frac{i}{2}(\varphi+\psi)}\cos\frac{\theta}{2} & e^{-\frac{i}{2}(\varphi-\psi)}\sin\frac{\theta}{2} \\ -e^{\frac{i}{2}(\varphi-\psi)}\sin\frac{\theta}{2} & e^{\frac{i}{2}(\varphi+\psi)}\cos\frac{\theta}{2} \end{bmatrix}. \tag{39}$$

This Jones matrix is the Kraus operator defining the quantum channel for a retarder. This channel is deterministic, so there is a single Kraus matrix.

2. Quantum channels for diattentuators

The different components of the electric field are differentially transmitted. For example, the transformations $h \to \sqrt{q}h$ and $v \to \sqrt{r}v$ correspond to transmission probabilities q and r for horizontally and vertically polarized light. This transformation is implemented by the diattenuator Mueller matrix M_d given in (31). A natural guess is that $\hat{a}_H \to \sqrt{q}\hat{a}_H$ and $\hat{a}_V \to \sqrt{r}\hat{a}_V$ provide the channel for a diattenuator. This simple transformation does not preserve the oscillator commutation relations. The paper[50] constructs the correct transformation by moving to an enlarged Hilbert space and then tracing out the auxiliary modes. The resulting Jones matrix is given by

$$J_d(\theta, \psi, r, q) = \frac{1}{2}\begin{bmatrix} \sqrt{q}+\sqrt{r}+(\sqrt{q}-\sqrt{r})\cos\theta & e^{i\psi}(\sqrt{q}-\sqrt{r})\sin\theta \\ e^{-i\psi}(\sqrt{q}-\sqrt{r})\sin\theta & \sqrt{q}+\sqrt{r}-(\sqrt{q}-\sqrt{r})\cos\theta \end{bmatrix}. \tag{40}$$

This provides the Kraus matrix needed to define the diattenuation channel. To achieve diattenuation along a different direction, apply a rotation followed by linear diattenuation and then the inverse of the original rotation. The rotation is parameterized by only two angles because only the direction of the diattenuation axis needs to be varied. Consequently, the four parameters of a general Mueller matrix representing diattenuation are captured by q, r, and the two angles specifying the diattenuation axis. Since this channel is deterministic, it involves a single Kraus matrix.

3. Quantum channels for depolarizers

Number conserving quantum operations account for the seven parameters of non-depolarizing Mueller matrices. The remaining nine free parameters are described by quantum operations that do not conserve photon number.[50] Any map from the space of density matrices back to the space of density matrices must

19 May 2025 14:12:42

© Author(s) 2025

be completely positive and trace-preserving (CPTP). The CPTP requirement enforces the known constraints for Mueller matrices, which were derived classically in Ref. 56. This strongly suggests a quantum-mechanical origin for the constraint that depolarizing Mueller matrices are formed from positive combinations of non-depolarizing Mueller matrices.[57] CPTP maps that transform Stokes operators into linear combinations of Stokes operators always allow a decomposition into convex combinations of CPTP maps corresponding to non-depolarizing Mueller matrices (since we study maps that do not mix different photon-number subspaces, the results of Ref. 56 validate this). In the single-photon subspace, the CPTP maps precisely match the classical constraint requiring convex combinations of non-depolarizing Mueller matrices. Therefore, convex combinations of the described channels are sufficient to represent all classical Mueller matrices. If the Kraus operators $\{\hat{K}_l^{(i)}\}$ correspond to Mueller matrix $M(i)$, then the quantum channel

$$\mathcal{E}(\hat{\rho}) = \sum_i p_i \sum_l \hat{K}(i)_l \hat{\rho} \hat{K}(i)_l^\dagger, \tag{41}$$

corresponds to the Mueller matrix

$$M = \sum_i p_i M(i). \tag{42}$$

It is a proven result that no more than four weights p_i are ever needed.[58]

This provides a complete description of the channels needed for a description of the polarization noise affecting photon B.

V. TOPOLOGICAL NOISE REJECTION

A central message of this study is that the skyrmion number demonstrates remarkable resilience in the presence of noise. In this section, we aim to build intuition for how this robustness emerges from encoding information into topological features, which are inherently sensitive only to the global structure of the wave function. The key idea is that noise tends to perturb local details, while topological invariants remain unchanged under such local distortions. Consequently, encoding information topologically offers a natural protection mechanism against noise. The arguments presented here are intended to provide conceptual insight and do not provide a formal proof of invariance under perturbations.

Topology is a systematic approach to characterizing quantities that are insensitive to smooth deformation. In our problem, this is the statement that the skyrmion number is unchanged by a change of coordinates $\vec{r}_A$ for photon A. To demonstrate this, start from the formula for the skyrmion number

$$N = \frac{1}{4\pi} \int_{-\infty}^{\infty} \int_{-\infty}^{\infty} \epsilon_{pqr} S_p \frac{\partial S_q}{\partial x} \frac{\partial S_r}{\partial y} dxdy, \tag{43}$$

and consider a smooth change of coordinates from x, y to $x' = x'(x,y)$ and $y' = y'(x,y)$. After some simple manipulations, we find the following transformation of the integrand:

$$\epsilon_{pqr} S_p \frac{\partial S_q}{\partial x} \frac{\partial S_r}{\partial y} = \left(\frac{\partial x'}{\partial x} \frac{\partial y'}{\partial y} - \frac{\partial y'}{\partial x} \frac{\partial x'}{\partial y} \right) \epsilon_{pqr} S_p \frac{\partial S_q}{\partial x'} \frac{\partial S_r}{\partial y'}.$$

The integration measure transforms as $dxdy = Jdx'dy'$, where the Jacobian is given by

$$J = \left(\frac{\partial x}{\partial x'} \frac{\partial y}{\partial y'} - \frac{\partial y}{\partial x'} \frac{\partial x}{\partial y'} \right) = \left(\frac{\partial x'}{\partial x} \frac{\partial y'}{\partial y} - \frac{\partial y'}{\partial x} \frac{\partial x'}{\partial y} \right)^{-1}.$$

Putting these transformation rules together, consequently

$$\begin{aligned} N &= \frac{1}{4\pi} \int_{-\infty}^{\infty} \int_{-\infty}^{\infty} \frac{1}{2} \epsilon_{pqr} S_p \frac{\partial S_q}{\partial x} \frac{\partial S_r}{\partial y} dxdy \\ &= \frac{1}{4\pi} \int_{-\infty}^{\infty} \int_{-\infty}^{\infty} \frac{1}{2} \epsilon_{pqr} S_p \frac{\partial S_q}{\partial x'} \frac{\partial S_r}{\partial y'} dx'dy', \end{aligned} \tag{44}$$

proving that the skyrmion number is independent of the choice of coordinates used for the calculation. This demonstrates that the skyrmion number remains invariant under smooth deformations, as any such deformation is effectively equivalent to a carefully selected change of coordinates. Consequently, the skyrmion number is perfectly robust against all sources of noise that can be modeled as a coordinate transformation.

This concept is illustrated in Fig. 2(a), where noise distorts the original skyrmion map, $\vec{S}(x,y)$, into a noisy map, $\vec{S}'(x,y)$, potentially altering the topology from N to N'. Since we are working with maps to unit spheres, S^2, we perform a normalization to ensure that $\vec{S}'(x,y) \cdot \vec{S}'(x,y) = 1$. After this normalization, we check whether a coordinate transformation (smooth deformation), $(x,y) \to (x',y')$, exists such that $\vec{S}'(x,y) \to \vec{S}(x',y')$. If such a transformation exists, then the noise is a smooth deformation, leaving the topology unchanged.

This intuitive argument can be formalized using the concept of homotopy. In topology, two continuous functions between topological spaces are said to be homotopic if one can be continuously deformed into the other. The continuous deformation connecting them is called a *homotopy*. More precisely, a homotopy between two continuous functions, $f(x)$ and $g(x)$, from a topological space X [represented as a loop in Fig. 2(b)] to a space Y (depicted as a deformed loop) is a continuous function $H : X \times [0,1] \to Y$ such that $H(x,0) = f(x)$ and $H(x,1) = g(x)$ for all $x \in X$. Since topological invariants—such as the skyrmion number—are preserved under homotopy, demonstrating robustness of our discrete signal against noise [denoted by $\hat{T}(\vec{s},t)$ in Fig. 2(c)] requires showing the existence of a homotopy between the noisy function, $\hat{T}(\vec{s},1)$, and the noise-free function, $\hat{T}(\vec{s},0)$. Coordinate transformations, which shuffle points in the domain of the map, represent a special class of smooth deformations. We have already shown that the skyrmion number remains invariant under such transformations, confirming invariance under this subset of homotopies. However, this class is limited in scope and does not encompass all possible homotopies. For instance, consider a constant field configuration: any reshuffling of domain points leaves the map unchanged, so in this case such transformations clearly cannot produce any non-trivial homotopies.[59] Therefore, coordinate transformations alone do not establish robustness against perturbations. To address this limitation, we adopt a two-pronged strategy. First, we explicitly demonstrate that the quantum channels modeling noise can be

19 May 2025 14:12:42

© Author(s) 2025

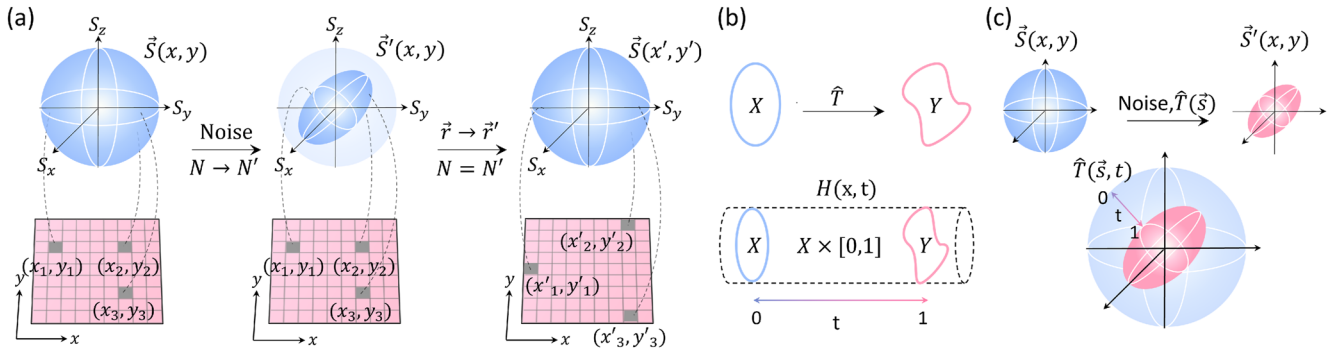


FIG. 2. Origin of topologically protected wave functions. (a) The map $\vec{S}(x,y)$ (left panel), derived from the skyrmion wave function, is a map from the plane to the sphere $R^2 \to S^2$. The map is distorted when the wave function is exposed to noise (middle panel), $\vec{S}(x,y) \to \vec{S}'(x,y)$. However, (right panel) if this distortion can be inverted with a smooth coordinate transformation $(x,y) \to (x',y')$, then the noise will not alter the topology of the state $N \to N' = N$, realizing topological protection. (b) To demonstrate that transformation $\hat{T}$ is a smooth deformation of topological space X into topological space Y, we construct a smooth homotopy $H(t,x)$ with $t \in [0,1]$ that enjoys the properties $H(0,x) = \mathbf{1}$ and $H(1,x) = \hat{T}$. (c) The noise channel distorts the initial map as $\hat{T}(\vec{S}(x,y)) = \vec{S}'(x,y)$. If this channel can be smoothly parameterized with parameter t such that $\hat{T}(0,\vec{S}(x,y)) = \vec{S}(x,y)$ is the identity and at $t = 1$, $\hat{T}(1,\vec{S}(x,y)) = \vec{S}'(x,y)$, then the noise channel induces a smooth deformation of the map defined by the skyrmion wave function, proving topological protection of the skyrmion topology.

continuously deformed into the identity channel, which trivially preserves the skyrmion number. Second, we substantiate this argument with numerical simulations that directly confirm the invariance of the skyrmion number in the presence of perturbations.

It is encouraging to note that in prior classical studies of vectorial light,[40] homotopy invariance has been successfully invoked to argue for noise resilience in a classical context. A key outcome of our work is the demonstration that these topological ideas extend naturally to the quantum regime. By explicitly constructing homotopies between noisy and noise-free density matrices, we establish the existence of a smooth deformation from the original quantum state to its noisy counterpart. This confirms that topological protection through homotopy invariance remains valid even at the full quantum level.

In the following analytic arguments, we restrict our analysis to noise parameters that vary smoothly with spatial coordinates (x,y). This assumption simplifies the derivations and allows for a more transparent theoretical treatment. However, this analytic approach does not address whether the skyrmion number remains resilient when the noise exhibits non-smooth or stochastic dependence on (x,y). To investigate this, we extend our analysis through numerical experiments, where we allow the noise parameters to acquire a stochastic spatial dependence. In all such cases, our results consistently demonstrate that the skyrmion number remains remarkably robust against the effects of noise.

A. Global considerations

The maps $\vec{S}(x,y)$ considered in this work are functions from $\mathbb{R}^2$ to S^2. A subtle but important omission in our earlier discussion is the lack of explicit specification of the topology assumed for $\mathbb{R}^2$. Two interpretations are logically consistent. One can work with the *compactified plane*—that is, $\mathbb{R}^2$ with a point added at infinity—which is topologically equivalent to S^2. Alternatively, one may work with the non-compact $\mathbb{R}^2$; in this case, the map is from a disk to a subset of S^2.

In our analysis, we adopt the compactified plane. This choice is motivated by the fact that, in this setting, the skyrmion number defines a bona fide topological invariant. Since we are studying homotopies of maps from S^2 to S^2, the skyrmion number is guaranteed to be integer-valued and invariant under smooth deformations. This is why it is conceptually advantageous to endow $\mathbb{R}^2$ with the topology of the sphere.

However, this choice comes with limitations. As discussed in Ref. 40, realistic noise can perturb the field configuration in such a way that compactification ceases to be valid. In such scenarios, the skyrmion number may fail to be homotopy invariant or integer-valued. In other words, the noise-induced deformation takes us outside the space of maps from S^2 to S^2, on which we focus.

Of course, adopting the compactified plane is not the only consistent approach. As emphasized in Ref. 40, one may instead work with the uncompactified plane, $\mathbb{R}^2$. The advantage of this approach is that any continuous deformation remains within the space of maps considered, so this discussion is general. However, the cost is that one no longer has a guarantee that the skyrmion number is an integer-valued, homotopy-invariant quantity. This property only holds when the homotopy on $\mathbb{R}^2$ descends to a homotopy on S^2, in which case the skyrmion number is an integer and homotopy invariant. If this descent fails, the skyrmion number is not in general homotopy invariant and will in general take non-integer values.

Ultimately, we have chosen to endow the plane with the topology of the sphere in order to clearly distinguish two effects: (1) local smooth deformations that preserve the space of maps from S^2 to S^2 and, therefore, the integer-valued topological invariant, and (2) global perturbations that can violate the topological structure and disrupt the quantization of the skyrmion number. For our purposes, this distinction is conceptually useful, as it isolates the role of topological protection from the effects of global breakdown. We will return to the latter in Sec. VIII.

19 May 2025 14:12:42

© Author(s) 2025

VI. TOPOLOGICAL PROTECTION AGAINST NON-DEPOLARIZING CHANNELS

The non-depolarizing channels are described by pure Mueller matrices, and they correspond to retarders and diattenuators. For pure Mueller matrices, there is a single term in the quantum channel. Topological invariance is established with a homotopy that interpolates between the original density matrix and the density matrix output of the quantum channel. For these channels, the Kraus operator is simply given by the Jones matrix associated with the Mueller matrix. The noise model of Sec. III allows the parameters of the Jones matrix to depend on position $\vec{r}_A$. Denote the space of $\vec{r}_A = (x, y)$ points $\mathbb{R}^2_A$, where A is for photon A. Denote the space of polarization states, the Poincaré sphere, as S^2_B, where B is for photon B.

The formula for the Stokes parameters (3) uses the diagonal matrix element of the density matrix with respect to the position space basis of photon A,

$$\hat{\rho}_B \equiv \langle \vec{r}_A|\psi\rangle\langle\psi|\vec{r}_A\rangle = \langle \vec{r}_A|\hat{\rho}|\vec{r}_A\rangle, \tag{45}$$

$\hat{\rho}_B$ is a 2×2 matrix and it is a density matrix in the sense that it is not negative

$$\langle v|\hat{\rho}_B|v\rangle \geq 0 \qquad \forall |v\rangle. \tag{46}$$

Furthermore, it is natural to normalize $\hat{\rho}_B$ at each point $\vec{r}_A$ since the Stokes parameters computed with the normalized $\hat{\rho}_B$ will be correctly normalized.

A. Retarder homotopy

A retarder is described using the Jones matrix given in (39). Notice that this Jones matrix is an element of SU(2). The angles φ, ψ, θ characterizing the retarder are all functions from $\mathbb{R}^2_A$ to the interval $[0, 2\pi]$. We now define the homotopy $H_R : \mathbb{R}^2_A \times [0, 1] \to \mathrm{SU}(2)$ as follows:

$$H_R(t, x, y) = \begin{bmatrix} e^{-\frac{i}{2}(\varphi_t+\psi_t)} \cos\frac{\theta_t}{2} & e^{-\frac{i}{2}(\varphi_t-\psi_t)} \sin\frac{\theta_t}{2} \\ -e^{\frac{i}{2}(\varphi_t-\psi_t)} \sin\frac{\theta_t}{2} & e^{\frac{i}{2}(\varphi_t+\psi_t)} \cos\frac{\theta_t}{2} \end{bmatrix}, \tag{47}$$

where $0 \leq t \leq 1$ and

$$\theta_t = t\theta(x, y) \qquad \varphi_t = t\varphi(x, y) \qquad \psi_t = t\psi(x, y). \tag{48}$$

Notice that $H_R(0, x, y) = \mathbf{1}$ and $H_R(1, x, y) = J_R(\theta, \varphi, \psi)$, where $\mathbf{1}$ is the 2×2 identity matrix and $J_R(\theta, \varphi, \psi)$ is the Jones matrix defined in (39). The $\sin(\cdot)$, $\cos(\cdot)$, and $e^{(\cdot)}$ functions are all infinitely differentiable; thus, as long as the functions defined in (48) are smooth functions of (x, y), we obtain a smooth homotopy from the undeformed state

$$H_R(0, x, y)\hat{\rho}_B H_R(0, x, y) = \hat{\rho}_B, \tag{49}$$

to the noisy state

$$H_R(1, x, y)\hat{\rho}_B H_R(1, x, y) = J_R(\theta, \varphi, \psi)\hat{\rho}_B J_R(\theta, \varphi, \psi)^\dagger. \tag{50}$$

Since every element in a connected Lie group can be smoothly deformed to the identity,[60] one might be tempted to conclude that the ability to deform the Kraus operator—represented by a Jones matrix implementing a rotation—to the identity follows trivially from the fact that SU(2) is a connected Lie group. However, this conclusion is not correct. The key point is that the Jones matrix depends on spatial coordinates x, y and, therefore, potentially defines a different element of SU(2) at each point in space. Constructing a homotopy in this context means building a smooth deformation of the entire map (i.e., the field of Jones matrices) to the identity matrix in such a way that smoothness with respect to x and y is preserved throughout the deformation. While each individual matrix may be deformable to the identity, global obstructions may prevent the existence of a single smooth homotopy that achieves this simultaneously across the full domain. This is precisely what must be addressed when demonstrating homotopy invariance in a spatially varying setting.[61] The continuous deformation to the identity given earlier is the homotopy establishing that the skyrmion number is unchanged by the action of a retarder. Furthermore, the existence of this smooth mapping demonstrates that this invariance is a consequence of topological noise rejection against the effects of retarders.

A comment is in order regarding the choice of the parameters $\theta(x, y)$, $\varphi(x, y)$, and $\psi(x, y)$. To illustrate the comment we wish to make, imagine we choose $\theta(x, y) = \tan^{-1}(y/x)$, aligning θ with the angular coordinate in polar coordinates on the plane. The function $t\theta(x, y) = t\ \tan^{-1}(y/x)$ is continuous in x and y only at $t = 0$ and $t = 1$. Continuity at $t = 1$ uses the fact that $\theta = 0$ and $\theta = 2\pi$ correspond to the same angular direction. On the other hand, the Jones matrix implementing the rotation is not continuous at $t = 1$. This is due to the fact that vectors at angles $\theta = \epsilon$ and $\theta = 2\pi - \epsilon$—which are close in angle—undergo vastly different rotations: the former rotates by a small amount, while the latter performs nearly a full 2π rotation. As a result, the Jones matrix is not continuous across $\theta = 0$ even though $\theta(x, y)$ is. To further support this claim, note that applying a rotation with $\theta(x, y) = \tan^{-1}(y/x)$ to a constant field configuration with skyrmion number zero produces a configuration with skyrmion number one. This discontinuous behavior indicates that such a transformation is not a homotopy of maps from $S^2 \to S^2$. To ensure a smooth deformation, one must require that nearby points undergo nearly identical rotations. This continuity condition ensures that the resulting deformation defines a sensible homotopy and rules out choices like $\theta(x, y) = \tan^{-1}(y/x)$.

It is worth noting that we can give an independent analytic demonstration of the independence of the skyrmion number against the effects of the retarder when the parameters of the retarder are constant. The Mueller matrix from the retarder, given in Eq. (30), shows that the retarder simply rotates the spatial components of the Stokes vector: $S_i \to \sum_j R_{ij}S_j$. The skyrmion number density therefore becomes

$$\sum_{ijk} \epsilon_{ijk} S_i \partial_x S_j \partial_y S_k \to \sum_{ijk}\sum_{lmn} \epsilon_{ijk} R_{il} R_{jm} R_{kn} S_l \partial_x S_m \partial_y S_n.$$

Now, use the identity

$$\sum_{ijk} \epsilon_{ijk} R_{il} R_{jm} R_{kn} = \det(R)\epsilon_{lmn} = \epsilon_{lmn}, \tag{51}$$

to conclude that the skyrmion number density is invariant under the action of the retarder.

19 May 2025 14:12:42

© Author(s) 2025

The analysis in this subsection demonstrates that, assuming the functions defined in (48) are smooth functions of (x,y), we can construct a smooth homotopy from the undeformed state to the noisy state. It is straightforward to test this conclusion numerically with a few conveniently chosen smooth functions. For this exercise, it proves useful to move to polar coordinates $x = \rho\cos\phi$ and $y = \rho\sin\phi$. Assume that the angle parameters of the retarder have the following coordinate dependence:

$$\begin{aligned}\theta &= \theta_0 e^{-\beta_1\rho^2}\cos(n_1\phi),\\ \varphi &= \varphi_0 e^{-\beta_2\rho^2}\cos(n_2\phi),\\ \psi &= \psi_0 e^{-\beta_3\rho^2}\cos(n_3\phi).\end{aligned} \tag{52}$$

Using the Jones matrix (39) as the Kraus matrix for a quantum channel, we can evaluate the skyrmion number after the channel is applied. When the angle parameters θ, φ, and ψ vanish, the Jones matrix evaluates to the identity. The constant parameters β_i for $i = 1,2,3$ control how rapidly the angle parameters fall to zero with increasing ρ so that the retarder acts in some local region centered on the origin $\rho = 0$. The constant parameters β_i for $i = 1,2,3$ control the spatial variation of the retarder parameters when ρ is fixed and ϕ is varied. Finally, the constant parameters θ_0, φ_0, and ψ_0 set the magnitude of the retarder angles. In this section and Sec. VI B, we will numerically evaluate the effect of different noise types on the skyrmion number of a given state. We note that deviations from the initial skyrmion number are expected due to two main factors: (1) the discretization of the component fields, $u_0^{l_i}$, of ρ_B and (2) the truncation of the integrand in Eq. (6) (further simulation details are given in the Appendix). Collectively, these two numerical factors lead to calculated skyrmion numbers with a slightly lower magnitude than the expected value. However, both factors can be mitigated by increasing the local pixel density (the number of pixels used to describe the field) as well as increasing the region of interest with respect to the Gaussian width, ω_0, of the fields at the cost of computational resources. Furthermore, it should be noted that the proceeding simulations do not account for additional errors that may arise in realistic scenarios due to the Poissonian statistics associated with single photon measurements, faulty detectors, etc. Such errors are best mitigated by appropriately choosing sufficient integration times, which may vary from one experimental configuration to the next, and ultimately map realistic experiments to the noise models studied in this work. Numerical results for various skyrmion topologies passed through a spatially varying retarder channel are shown in Fig. 3. In Fig. 3(a), the initial map $\vec{S}(x,y)$ with a skyrmion number of $N = 1$ is shown as a covered sphere with regions of interest (ROIs) highlighted and correlated by color to the corresponding ROIs in the plane. After passing the state through a spatially varying retarder, $\vec{S}(x,y)$ is transformed to $\vec{S}'(x,y)$. The only effect of this transformation is a rotation of the Stokes vectors as indicated by the shift in position of the ROIs on the sphere. Importantly, the full coverage of the sphere is maintained, thus leaving the skyrmion number unaltered, as shown in Fig. 3(b). Numerical results for states possessing skyrmion numbers $N = \{-3,-2,-1,1,2,3\}$ before (initial) and after (final) they were passed through the spatially varying retarder channel are shown. From these results it is clear that the initial state's topology is invariant under the action of the spatially varying retarder, thus confirming that the skyrmion number is invariant for the above ρ,ϕ dependence of the retarder parameters, in agreement with the homotopy construction.

B. Diattenuator homotopy

The channel corresponding to a diattenuator has a Kraus matrix given by the Jones matrix in (40). The channel parameters are angles θ,ψ, which are functions from $\mathbb{R}_A^2$ to the interval $[0,2\pi)$, as well as the non-negative parameters q,r, which are functions from $\mathbb{R}_A^2$ to $(0,1)$. We now define the homotopy $H_d : \mathbb{R}_A^2 \times [0,1] \to \mathrm{SU}(2)$ as follows:

$$H_d(t,x,y) = \frac{1}{2}\begin{bmatrix}\sqrt{q_t}+\sqrt{r_t}+(\sqrt{q_t}-\sqrt{r_t})\cos\theta_t & e^{i\psi_t}(\sqrt{q_t}-\sqrt{r_t})\sin\theta_t\\ e^{-i\psi_t}(\sqrt{q_t}-\sqrt{r_t})\sin\theta_t & \sqrt{q_t}+\sqrt{r_t}-(\sqrt{q_t}-\sqrt{r_t})\cos\theta_t\end{bmatrix}, \tag{53}$$

where $0 \le t \le 1$ and

$$\begin{aligned}\theta_t &= t\theta(x,y), & \psi_t &= t\psi(x,y),\\ q_t &= (1-t)+tq, & r_t &= (1-t)+tr.\end{aligned} \tag{54}$$

This homotopy obeys $H_d(0,x,y) = \mathbf{1}$ and $H_d(1,x,y) = J_d(\theta,\psi,r,q)$, where $\mathbf{1}$ is the 2×2 identity matrix and $J_d(\theta,\psi,r,q)$ is the Jones matrix defined in (40). The $\sin(\cdot)$, $\cos(\cdot)$, and $e^{(\cdot)}$ functions are all infinitely differentiable, so as long as the functions defined in (54) are smooth functions of (x,y). The $\sqrt{(\cdot)}$ functions have square root branch points when their argument vanishes, so they are not analytic (i.e., smooth) at these points. It is, however, clear that this singularity is only reached for $t = (1-r)^{-1}$ or for $t = (1-q)^{-1}$. Since both r and q are less than 1, we never reach these singularities. Therefore, we obtain a smooth homotopy from the undeformed state

$$H_d(0,x,y)\hat{\rho}_B H_d(0,x,y) = \hat{\rho}_B, \tag{55}$$

to the noisy state

$$H_d(1,x,y)\hat{\rho}_B H_d(0,x,y) = J_d(\theta,\psi,r,q)\hat{\rho}_B J_d(\theta,\psi,r,q)^\dagger. \tag{56}$$

This proves that the skyrmion number is resilient against the effects of a diattenuator and that topological noise rejection is the mechanism behind this resilience.

We have argued that, under the assumption that the functions defined in (54) are smooth functions of (x,y), we obtain a smooth homotopy from the undeformed state to the noisy state. We

19 May 2025 14:12:42

© Author(s) 2025

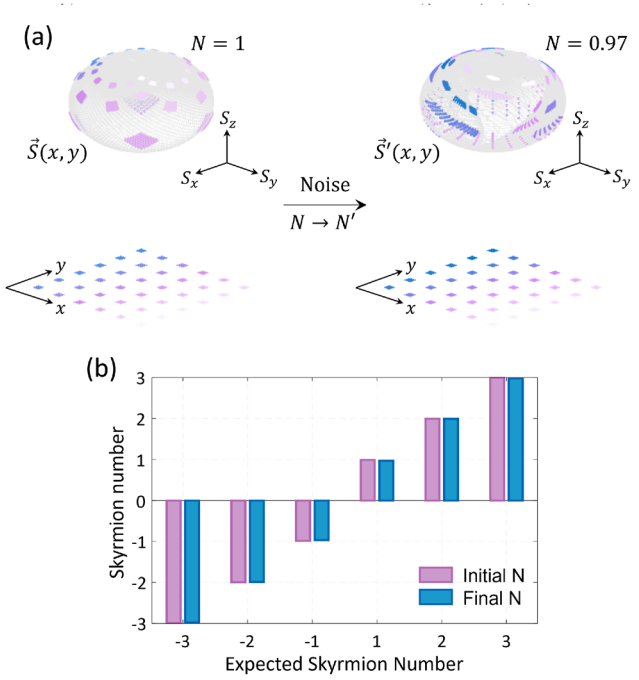


FIG. 3. Skyrmion resilience against the retarder channel. (a) Skyrmion map for $N = 1$ shown before (left panel) and after (right panel) passing through a spatially varying retarder channel. Although the mapping is altered, $\vec{S}(x,y) \to \vec{S}'(x,y)$, the net effect is a shifting of points on the sphere without changing the wrapping number. Indeed, the calculated skyrmion number for the noisy signal is $N \approx 0.97$. To illustrate the movement of points under the influence of noise, we have color-coded regions of interest on the plane and the sphere. These points can be returned to their original configuration by transforming points in the plane, i.e., $\vec{S}(x,y) \to \vec{S}'(x,y) \to \vec{S}(x',y')$. This explains why the skyrmion number is robust. (b) Numerically calculated skyrmion number before (initial) and after (final) passing the state through the noisy channel, compared to the expected skyrmion number for various topologies $N \in \{-3,-2,-1,1,2,3\}$. The plot demonstrates the invariance of the topology under the influence of the spatially varying retarder channel.

can again test this conclusion numerically with conveniently chosen smooth functions for the channel parameters. The functions we use are given by

$$\begin{aligned} \theta &= \theta_0 e^{-\beta_1 \rho^2} \cos(n_1 \phi), \\ \psi &= \psi_0 e^{-\beta_2 \rho^2} \cos(n_2 \phi), \\ q &= (1 - e^{-\beta_3 \rho^2} \cos(n_3 \phi)), \\ r &= (1 - e^{-\beta_4 \rho^2} \cos(n_4 \phi)). \end{aligned} \tag{57}$$

As $\rho \to \infty$, the channel parameters assume the limit values $\theta = 0 = \psi$ and $q = 1 = r$. At these limiting values, the Jones matrix (40) reduces to the two dimensional unit matrix, and the channel acts trivially. The constant parameters β_i for $i = 1,2,3,4$ control how rapidly these limiting values are attained as ρ increases. Therefore, with this choice of functions, the channel again acts non-trivially in a finite region centered on $\rho = 0$. The constant parameters n_i for $i = 1,2,3,4$ control the spatial variation of the channel parameters at fixed ρ as ϕ is varied. Finally, the constant parameters θ_0 and ψ_0 set the magnitude of the two angles defining the diattenuator. Using the Jones matrix (40) as the Kraus matrix for a quantum channel, with the above spatially varying channel parameters, it is simple to evaluate the skyrmion number after the channel acts. Numerical results for various skyrmion topologies after the action of a spatially varying diattenuator channel are presented in Fig. 4. In Fig. 4(a), the initial map $\vec{S}(x,y)$ with a skyrmion number of $N = 1$ is transformed into $\vec{S}'(x,y)$. This transformation induces a rotation of the Stokes vectors, as shown by the shift in the position of the ROIs on the sphere. Despite this shift, the full coverage of the sphere is preserved, leaving the skyrmion number virtually unchanged, with $N \approx 0.99$. Figure 4(b) shows the numerical results for states with skyrmion numbers $N = \{-3,-2,-1,1,2,3\}$ before (initial) and after (final) passing through the spatially varying diattenuator channel. These results demonstrate that the topology of the initial state is unaltered, confirming that the skyrmion number is invariant under the specific ρ, ϕ dependence chosen for the diattenuator parameters, in agreement with the homotopy construction.

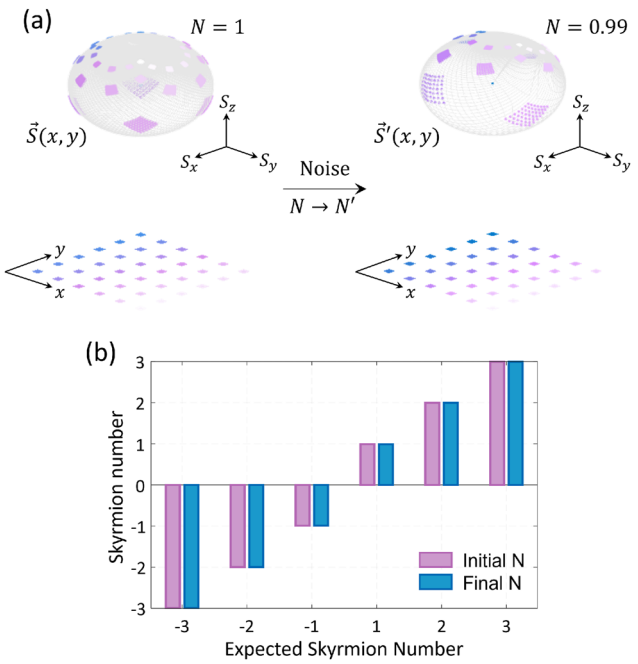


FIG. 4. Skyrmion resilience to diattenuator channel. (a) Skyrmion map for $N = 1$ before (left panel) and after (right panel) passing through a spatially varying diattenuator channel. While the mapping is altered, $\vec{S}(x,y) \to \vec{S}'(x,y)$, points on the sphere merely shift without changing the wrapping number, leaving the skyrmion number intact at $N \approx 0.99$. This is highlighted by color-matching correlated regions of interest on the plane with those on the sphere, illustrating that the shifts on the sphere can be compensated for using a transformation of the plane, i.e., $\vec{S}(x,y) \to \vec{S}'(x,y) \to \vec{S}(x',y')$. (b) Numerically calculated skyrmion numbers (before and after passing the state through the noisy channel) compared to expected skyrmion numbers for various topologies, $N \in \{-3,-2,-1,1,2,3\}$. The results show clear invariance of the topology to the spatially varying diattenuator channel.

19 May 2025 14:12:42

© Author(s) 2025

VII. DEPOLARIZING CHANNELS

The depolarizing channels are realized as more general CPTP maps, which necessarily involve a sum over multiple Kraus operators. This requires an extension of the formalism developed in Sec. VI B, as we now explain. Each term in the sum contributes to the overall noise affecting the density matrix. To establish a smooth deformation between the noisy and noise-free density matrices, it is necessary to construct a homotopy for each term in the sum. However, even if such a collection of homotopies exists, it is not sufficient to fully describe the interference effects between different Kraus operators. The challenge arises from the non-linear dependence of the skyrmion number on the Stokes parameters. While the Stokes parameters, as defined in (3), are linear in the density matrix, the skyrmion number (6) is cubic in the Stokes parameters. This implies that different Kraus terms interfere in a non-trivial way, making it insufficient to consider homotopies independently for each term.

Consider the noisy density matrix $\hat{\rho}_{noisy}$ resulting from the application of n_C quantum channels,

$$\hat{\rho}_{noisy} = \sum_{i=1}^{n_C} E_i \hat{\rho} E_i^\dagger \equiv \sum_{i=1}^{n_C} p_i \hat{\rho}_i, \tag{58}$$

where the coefficients p_i are positive and satisfy $\sum_{i=1}^{n_C} p_i = 1$. Each channel density matrix $\hat{\rho}_i$, as well as the total density matrix $\hat{\rho}_{\text{noisy}}$, has unit trace. Consequently, the Stokes parameters associated with each channel

$$\tilde{S}_j^{(i)}(\vec{r}_A) = \mathrm{Tr}_B\big(\langle \vec{r}_A|\hat{\rho}_i|\vec{r}_A\rangle \sigma_{Bj}\big), \tag{59}$$

and those associated with the total density matrix

$$\tilde{S}_j(\vec{r}_A) = \mathrm{Tr}_B\big(\langle \vec{r}_A|\hat{\rho}_{\text{noisy}}|\vec{r}_A\rangle \sigma_{Bj}\big), \tag{60}$$

are correctly normalized,

$$\vec{\tilde{S}}^{(i)}(\vec{r}_A)\cdot\vec{\tilde{S}}^{(i)}(\vec{r}_A) = 1, \quad \vec{\tilde{S}}(\vec{r}_A)\cdot\vec{\tilde{S}}(\vec{r}_A) = 1. \tag{61}$$

The total Stokes parameters are related to the individual channel contributions via

$$\vec{\tilde{S}}(\vec{r}_A) = \sum_{i=1}^{n_C} p_i\, \vec{\tilde{S}}^{(i)}(\vec{r}_A). \tag{62}$$

Several of the noise channels discussed below induce discrete transformations on the Stokes parameters. For example, the bit-flip and phase-flip channels generate the following transformations:

$$\begin{aligned} &\tilde{S}_x \to \tilde{S}_x, \quad \tilde{S}_y \to -\tilde{S}_y, \quad \tilde{S}_z \to -\tilde{S}_z, \\ &\tilde{S}_x \to -\tilde{S}_x, \quad \tilde{S}_y \to -\tilde{S}_y, \quad \tilde{S}_z \to \tilde{S}_z. \end{aligned} \tag{63}$$

A model incorporating bit-flip and phase-flip channels, with position-dependent channel parameters, results in the transformation

$$\begin{aligned} \tilde{S}_x &\to (1-2p^{\text{phase flip}})\tilde{S}_x, \\ \tilde{S}_y &\to (1-2p^{\text{phase flip}}-2p^{\text{bit flip}})\tilde{S}_y, \\ \tilde{S}_z &\to (1-2p^{\text{bit flip}})\tilde{S}_z. \end{aligned} \tag{64}$$

This transformation effectively deforms the sphere into an ellipsoid, a process that preserves the winding number. A closely analogous argument applies to the depolarizing channel induced by isotropic noise. In this case, the noise introduces a mixed term in the density matrix, proportional to the identity matrix, with a magnitude determined by the noise strength. Consequently, the entangled components of the density matrix are reduced, leading to a uniform rescaling of the Stokes parameters, which in turn shrinks the sphere. Since this transformation does not alter the topological structure, the wrapping number remains unchanged.

The noise channels discussed earlier all reduce to a scaling of the components of the Stokes vector. Consequently, while interference terms are non-zero, their cumulative effect is merely an overall normalization factor, which does not alter the wrapping number. We now turn to more intricate models in which, for example, the components of the Stokes vector may be permuted among one another. Toward this end, recall that our wave function (1) leads to the Stokes vector,

$$\begin{aligned} S_x &= 2^{\frac{|l_1|+|l_2|+2}{2}}\cos\big(\phi(l_1-l_2)\big)\rho^{|l_1|+|l_2|}w_0^{-|l_1|-|l_2|-2}\frac{e^{-\frac{2\rho^2}{w_0^2}}}{\pi\sqrt{|l_1|!|l_2|!}}, \\ S_y &= 2^{\frac{|l_1|+|l_2|+2}{2}}\sin\big(\phi(l_1-l_2)\big)\rho^{|l_1|+|l_2|}w_0^{-|l_1|-|l_2|-2}\frac{e^{-\frac{2\rho^2}{w_0^2}}}{\pi\sqrt{|l_1|!|l_2|!}}, \\ S_z &= e^{-\frac{2\rho^2}{w_0^2}}w_0^{-2(|l_1|+|l_2|+1)}\frac{2^{|l_2|}|l_1|!w_0^{2|l_1|}\rho^{2|l_2|}-\left(2^{|l_1|}|l_2|!\rho^{2|l_1|}w_0^{2|l_2|}\right)}{\pi|l_1|!|l_2|!}. \end{aligned} \tag{65}$$

A discrete transformation mapping $\{S_x, S_y, S_z\}$ into either $\{S_y, S_x, S_z\}$ or $\{S_z, S_y, S_x\}$ cannot be modeled as a simple rescaling of the Stokes parameters. Using relation (62), the topological number density is given by

$$\Sigma_z(x,y) = \sum_{i,j,k=1}^{n_C}\sum_{p,q,r=1}^{3}\tilde{S}_p^{(i)}\frac{\partial\tilde{S}_q^{(j)}}{\partial x}\frac{\partial\tilde{S}_r^{(k)}}{\partial y}. \tag{66}$$

The diagonal terms ($i = j = k$) capture contributions from individual channels, whereas the off-diagonal terms encode interference effects between different channels. The resilience of the diagonal terms follows, as argued in Sec. VI B, if a homotopy can be established for each channel. For now, we assume the existence of such a homotopy and focus our attention on the interference terms.

For the interference terms to contribute a non-zero wrapping number, the evolution of the three components of the Stokes vector must be carefully choreographed. Random oscillations of these components will initially induce winding, only to later unwind, and so forth, ultimately canceling out. Indeed, the S_x component of (65) depends on $\cos\big(\phi(l_1-l_2)\big)$, while S_y depends on $\sin\big(\phi(l_1-l_2)\big)$. As ϕ varies, the signs of these two components are correlated in such a way that the tip of the Stokes vector orbits the origin $l_1 - l_2$ times. However, in the presence of noise, such oscillations will generally be randomized, leading to an overall vanishing winding number.

To illustrate this, consider a simple model consisting of an identity channel (with probability p) and a second channel that swaps S_x and S_y, i.e., $\{S_x, S_y, S_z\} \to \{S_y, S_x, S_z\}$, with probability $1-p$. One potential interference term involves the selection $\{S_x^{(1)}, S_y^{(2)}, S_z^{(1)}\}$.

19 May 2025 14:12:42

© Author(s) 2025

Since both $S_x^{(1)}$ and $S_y^{(2)} = S_x^{(1)}$ vary with ϕ as $\cos(\phi(l_1 - l_2))$, the tip of the Stokes vector first winds and then unwinds, resulting in a net wrapping number of zero. A direct evaluation using this triple confirms that the skyrmion number vanishes. Moreover, selecting other off-diagonal triples does not alter this conclusion, reinforcing the idea that uncoordinated oscillations suppress non-trivial topological contributions.

The arguments presented earlier are not rigorous but serve to build intuition regarding the resilience of the skyrmion number to depolarizing channels. To establish this claim more definitively, we employ numerical methods to analyze the impact of depolarizing channels on the skyrmion number. For a comprehensive investigation, we consider the full set of quantum channels listed in Ref. 46. Our numerical results consistently demonstrate that the skyrmion number exhibits remarkable robustness against the introduction of depolarizing noise.

Our goal is to model the most general source of noise experienced by the abstract qubit with states $|H\rangle_B$, $|V\rangle_B$. The channels described in Ref. 46 have been shown to be relevant for the description of depolarization of qubits. Typically, these models use decoherence to model the decorrelation that occurs during depolarization. While decoherence is usually accompanied by dissipation, depolarization specifically considers pure decoherence (or dephasing), where energy dissipation is negligible. In the terminology of Ref. 46, the resulting depolarizing channel is a decoherence process induced by unbiased noise generating bit-flip and phase-flip errors.

A. Bit flip channel

The bit flip channel is described by the operators

$$E_0 = \sqrt{p}\begin{pmatrix}1 & 0\\ 0 & 1\end{pmatrix} \qquad E_1 = \sqrt{1-p}\begin{pmatrix}0 & 1\\ 1 & 0\end{pmatrix}, \tag{67}$$

which obey $E_0^\dagger E_0 + E_1^\dagger E_1 = \mathbf{1}$ with $\mathbf{1}$ the 2×2 identity matrix. With a probability p, states $|H\rangle$ and $|V\rangle$ remain what they are, and with a probability $1-p$, they are swapped. To get a local model, we must allow p to be a smooth function of x and y. Note that $0 \le p \le 1$. A simple choice for p is

$$p = (\alpha + \beta\cos(n\phi))e^{-\gamma\rho^2}, \tag{68}$$

where we have again employed polar coordinates. As $\rho \to \infty$, we find that $p \to 0$. The constant parameter γ controls how quickly p approaches 0. At $p = 0$, the states H and V are swapped so that this channel is not confined to a local region but rather continues to have an effect even at $\rho = \infty$. Acting on the Stokes parameters, this channel takes

$$S_x \to S_x \quad S_y \to -S_y \quad S_z \to -S_z, \tag{69}$$

at large ρ where $p = 0$. It is simple to see that the skyrmion number is invariant under this transformation. The constant parameters α and β are needed, with $\alpha > \beta$, to enable p to oscillate but remain positive. The constant parameter n controls this oscillatory behavior as ϕ is varied for fixed ρ. We only consider integer n. For the above choice of p, we can easily evaluate the action of the channel on the density matrix. Using the noisy density matrix, we have numerically verified that the skyrmion number is robust against the polarization flip channel.

There is an interesting point that deserves discussion. Taking p constant, we find the Stokes parameters, before normalization, are given by

$$\begin{aligned}
S_x &= 2^{\frac{|l_1|+|l_2|}{2}}\left(1 + e^{2i\phi(l_1-l_2)}\right)\rho^{|l_1|+|l_2|} \\
&\quad \times w_0^{-|l_1|-|l_2|-2}\frac{e^{-\frac{2\rho^2}{w_0^2}-i\phi(l_1-l_2)}}{\pi\sqrt{|l_1|!|l_2|!}}, \\
S_y &= i(2p-1)2^{\frac{|l_1|+|l_2|}{2}}\left(e^{2i\phi(l_1-l_2)} - 1\right)\rho^{|l_1|+|l_2|} \\
&\quad \times w_0^{-|l_1|-|l_2|-2}\frac{e^{-\frac{2\rho^2}{w_0^2}-i\phi(l_1-l_2)}}{\pi\sqrt{|l_1|!|l_2|!}}, \\
S_z &= (2p-1)e^{-\frac{2\rho^2}{w_0^2}}w_0^{-2(|l_1|+|l_2|+1)} \\
&\quad \times \frac{\left(2^{|l_1|}|l_2|!\rho^{2|l_1|}w_0^{2|l_2|} - 2^{|l_2|}|l_1|!w_0^{2|l_1|}\rho^{2|l_2|}\right)}{\pi|l_1|!|l_2|!}.
\end{aligned} \tag{70}$$

It is clear that choosing $p = \frac{1}{2}$, we have $S_y = S_z = 0$, and the skyrmion number vanishes. Therefore, for a constant $p = \frac{1}{2}$, the skyrmion number is completely destroyed. The reason for this anomalous behavior is simply that for $p = \frac{1}{2}$, the channel sums the original density matrix with the density matrix obtained by swapping $|V\rangle$ and $|H\rangle$. This obviously renders the density matrix symmetric so that it admits a decomposition

$$\hat{\rho} = \frac{1}{2}\sigma_0 + c_1\sigma_1, \tag{71}$$

with one undetermined coefficient c_1. From formula (3), it is now apparent why both S_y and S_z vanish. It is also clear that this does not happen at any other value of $p \neq \frac{1}{2}$. Pertinent to this is how likely it is that realistic conditions might result in exactly $p = \frac{1}{2}$? First, we can anticipate that the value of p will fluctuate. Second, note that the isolated points or even lines when $p = \frac{1}{2}$ are all lower dimensional (0-dimensional or 1-dimensional) compared to the set (2-dimensional) we are integrating over, so they are all sets of measure zero. Changing an integrand on a set of measure zero will not affect the value of an integral. These theoretical and practical considerations lead us to surmise that this $p = \frac{1}{2}$ anomalous behavior will not play any role, and consequently that the skyrmion number will remain robust in such channels.

Further numerical results for various skyrmion topologies passed through both constant and spatially varying bit-flip channels are presented in Figs. 5 and 6, respectively. In Fig. 5(a), the initial map $\vec{S}(x,y)$ with a skyrmion number $N = 1$ undergoes transformation to $\vec{S}'(x,y)$ after passing through a bit-flip channel with a noise probability of $p = 0.35$. This introduces noticeable distortion in the spherical geometry of $\vec{S}(x,y)$, as the S_y and S_z components are scaled by a factor of $1-2p$, giving the geometry an elliptical appearance. However, following a renormalization to ensure $\vec{S}'(x,y)\cdot\vec{S}'(x,y) = 1$, we observe that the noise-induced transformation simply rotates the Stokes vectors, shifting the regions of interest (ROIs) on the sphere without altering the overall coverage. Consequently, the skyrmion number remains unchanged at $N \approx 0.97$. Figure 5(b) shows the numerical results for initial and final states possessing

19 May 2025 14:12:42

© Author(s) 2025

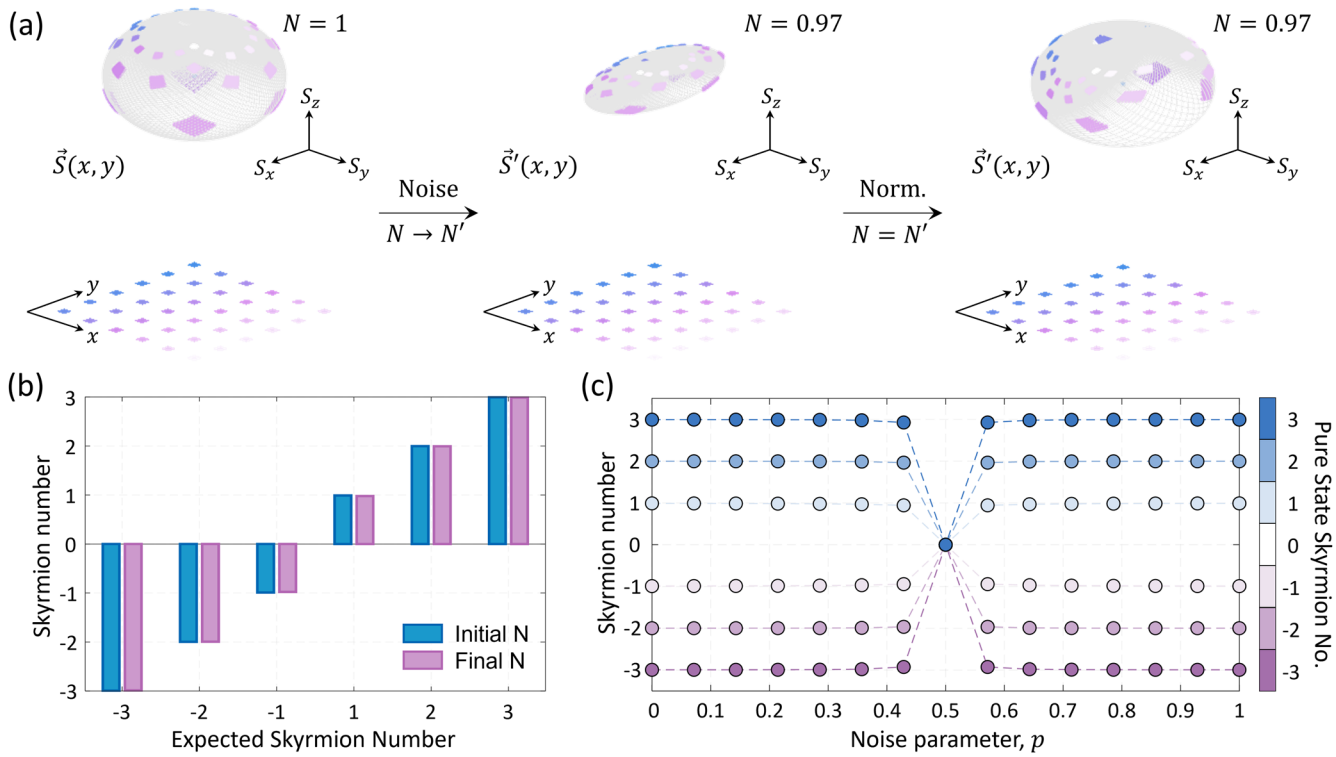


FIG. 5. Skyrmion resilience against constant bit-flip channels. (a) Skyrmion map for $N = 1$ before (left panel) and after (middle panel) passing through a constant bit-flip channel with noise parameter $p = 0.35$. The mapping is visibly distorted, $\vec{S}(x,y) \to \vec{S}'(x,y)$. To properly evaluate the skyrmion number, $\vec{S}'(x,y)$ is normalized (right panel) such that $\vec{S}'(x,y) \cdot \vec{S}'(x,y) = 1$. The distortion due to noise is a simple shifting of points on the sphere that preserves the wrapping number, so that the calculated skyrmion number is $N \approx 0.97$. This is highlighted by matching colors to correlate regions of interest on the plane with those on the sphere, emphasizing that the movement of points on the sphere can be corrected by a coordinate transformation of the plane, i.e., $\vec{S}(x,y) \to \vec{S}'(x,y) \to \vec{S}(x',y')$. (b) Numerically calculated skyrmion numbers before and after passing through the noisy channel ($p = 0.35$) for various topologies, $N \in \{-3,-2,-1,1,2,3\}$, demonstrate clear invariance of the topology to the bit-flip channel. (c) The calculated skyrmion number plotted against the noise parameter p shows the robustness of the topology across all bit-flip noise settings, with the only exception occurring at $p = 0.5$, where entanglement is completely lost.

skyrmion numbers $N \in \{-3,-2,-1,1,2,3\}$ after passing through the same constant bit-flip channel, while Fig. 5(c) explores these results across various bit-flip noise settings. The data reveal that the topology remains fully invariant to bit-flip noise, with the skyrmion number only vanishing at the singular limit of $p = 0.5$. At this limit, the state becomes unentangled, and by definition, $N = 0$. Intuitively, we find that at $p = 0.5$, $S_y = S_z = 0$, meaning that after renormalization, $\vec{S} = [1,0,0]^T$ for all positions (x,y), so that the initial topology has been lost. In Fig. 6(a), numerical results illustrate the distortion of $\vec{S}(x,y)$ with $N = 1$ as it passes through a spatially varying bit-flip channel with a spatially dependent noise parameter, $p(x,y)$, defined by (68). Although the new map $\vec{S}'(x,y)$ parametrizes a highly distorted geometry relative to the original spherical form, the initial skyrmion number of $N \approx 0.99$ is preserved, as expected, due to the smooth spatial dependence of the noise. Figure 6(b) confirms this robustness across different topological numbers passed through the same noise channel, demonstrating that skyrmion topology remains invariant under both varying noise levels and spatially dependent noise.

B. Phase flip channel

The phase flip channel is described by the operators

$$E_0 = \sqrt{p}\begin{pmatrix} 1 & 0 \\ 0 & 1 \end{pmatrix}, \qquad E_1 = \sqrt{1-p}\begin{pmatrix} 1 & 0 \\ 0 & -1 \end{pmatrix}, \tag{72}$$

which obey $E_0^\dagger E_0 + E_1^\dagger E_1 = \mathbf{1}$ with $\mathbf{1}$ the 2×2 identity matrix and again we must allow p to be a smooth function of x and y. It is again useful to consider the simple choice (68). With this choice, our numerical results confirm that the skyrmion number is robust against noise introduced by the phase flip channel.

In Subsection VII A, we found that the bit flip channel with the specific parameter choice $p = \frac{1}{2}$ completely destroyed the skyrmion number, reducing it to zero. There is a similar result for the phase flip channel: choosing $p = \frac{1}{2}$, we have $S_x = S_y = 0$, and the skyrmion number vanishes. Just as for the bit flip channel, even though the parametrization (68) leads to $p = \frac{1}{2}$ at some isolated points or even

19 May 2025 14:12:42

© Author(s) 2025

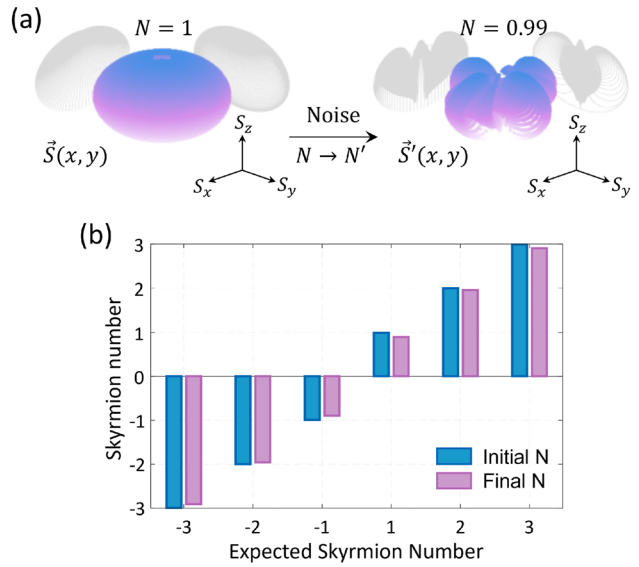


FIG. 6. Skyrmion resilience against a spatially varying bit-flip channel. (a) Skyrmion map for $N = 1$ before (left panel) and after (right panel) passing through a spatially varying bit-flip channel. Although the mapping is significantly distorted, $\vec{S}(x,y) \to \vec{S}'(x,y)$, the calculated skyrmion number remains close to the expected value at $N \approx 0.99$, indicating that the topology is preserved despite the deformation. To aid in visualization, the point clouds representing $\vec{S}(x,y)$ and $\vec{S}'(x,y)$ have been plotted with a color gradient indicating the change in S_z and S_z'. Furthermore, projections onto the planes $S_x - S_z$ and $S_y - S_z$ were performed on both maps, shown as gray shadows, further highlighting the distortion caused by noise. This visualization is repeated overall for the spatially varying channels that follow. (b) Numerically calculated skyrmion numbers for various topologies, $N \in \{-3, -2, -1, 1, 2, 3\}$, before and after passing through the spatially varying bit-flip channel, demonstrating the clear invariance of the topology even under spatially dependent bit-flip noise.

lines, these bad values do not disturb the skyrmion number under realistic situations: once again, in practice the value of p will fluctuate, so we do not expect that this $p = \frac{1}{2}$ anomalous behavior will play any role.

Further numerical results for various skyrmion topologies passed through constant and spatially varying phase-flip channels are shown in Figs. 7 and 8, respectively. In Fig. 7(a), the initial map $\vec{S}(x,y)$, with skyrmion number $N = 1$, is passed through a phase-flip channel with noise parameter $p = 0.35$ to give the noisy $\vec{S}'(x,y)$ signal. This channel induces a noticeable distortion in the spherical geometry of the initial wave function. This is as expected, as the S_x and S_y components are scaled by a constant factor of $1 - 2p$, giving the appearance of an elliptical deformation. However, after renormalizing the Stokes parameters so that $\vec{S}'(x,y) \cdot \vec{S}'(x,y) = 1$, it is evident that the noise simply rotates the Stokes vectors. Consequently, the coverage of the sphere is intact and the skyrmion number is preserved. In Fig. 7(b), numerical results for skyrmion numbers $N \in \{-3, -2, -1, 1, 2, 3\}$, before and after passing through the constant phase-flip channel, show that the topology is unchanged. Figure 7(c) illustrates this invariance across a range of phase-flip noise settings. The topology is unaffected by phase-flip noise, except at the critical point $p = 0.5$, where the entanglement vanishes, and by definition, $N = 0$. Intuitively, at this point, $S_x = S_y = 0$, and after renormalization, $\vec{S} = [0, 0, 1]^T$ for all positions (x, y), indicating a complete collapse of the original topology. In Fig. 8(a), numerical results illustrate the deformation of $\vec{S}(x,y)$ with $N = 1$ after passing through a spatially varying phase-flip channel, where the noise parameter $p(x,y)$ is defined according to (68). Despite the apparent significant distortion of the geometry of the wave function when compared to the initial state, the skyrmion number is intact at $N \approx 0.99$, as expected for a noise parameter that varies smoothly with changing values of the spatial coordinates. Figure 8(b) presents results for different topological numbers passed through the same spatially varying noise channel, confirming the complete robustness of the skyrmion topology to phase-flip noise across different noise levels and spatial variations.

C. Depolarizing channel

The depolarizing channel is described by the quantum operation $(0 \le p \le 1)$,

$$\mathcal{E}(\hat{\rho}) = \frac{p}{2}\mathbf{1} + (1 - p)\hat{\rho}. \tag{73}$$

This channel is very similar to the case of isotropic noise considered in Ref. 42. The present analysis generalizes the discussion of Ref. 42 since we allow p to be a smooth function of x and y. Since our density matrix lives in the tensor product of a two dimensional polarization Hilbert space, with a two dimensional position Hilbert space we must be careful to choose the coefficient of the term $\mathbf{1}$ in such a way that our state remains normalizable. A suitable choice is to take p to be of the form

$$p(\rho, \phi) = (\alpha + \beta \cos(n\phi)) \exp\left(-\gamma\rho^2\right), \tag{74}$$

with α and β chosen to ensure that $0 < p \le 1$. With the above choice, we find that $p \to 0$ as $\rho \to \infty$ so that the channel acts in a local region centered on $\rho = 0$. The parameter n controls how p fluctuates at fixed ρ as ϕ is varied. We assume that n is an integer. Our numerical results confirm that the skyrmion number is completely robust to the depolarizing channel. The discussion is exactly as in Ref. 42. That analysis proves that the depolarizing channel induces a smooth deformation of the skyrmion state that leaves the topology unchanged. The topology only collapses when the state is maximally mixed and no entanglement remains.

In the depolarizing channel, the density matrix is perturbed by a maximally mixed state, which corresponds to adding a term proportional to the identity. This maximally mixed term gives a vanishing contribution to the Stokes parameters, so that in the end the net effect is to multiply the Stokes parameters by an overall constant. This change in the magnitude of the Stokes vector is a smooth deformation of the Stokes parameters, so that for this channel it is also possible to give a homotopy between the noisy and noise-free Stokes parameters. This is the only depolarizing channel we have considered that admits a homotopy analysis. The reason why the homotopy analysis continues to be useful is simply that the maximally mixed term [i.e., the term on the RHS of (73) proportional to $\mathbf{1}$] gives a vanishing contribution to the Stokes parameters, so there are no

19 May 2025 14:12:42

© Author(s) 2025

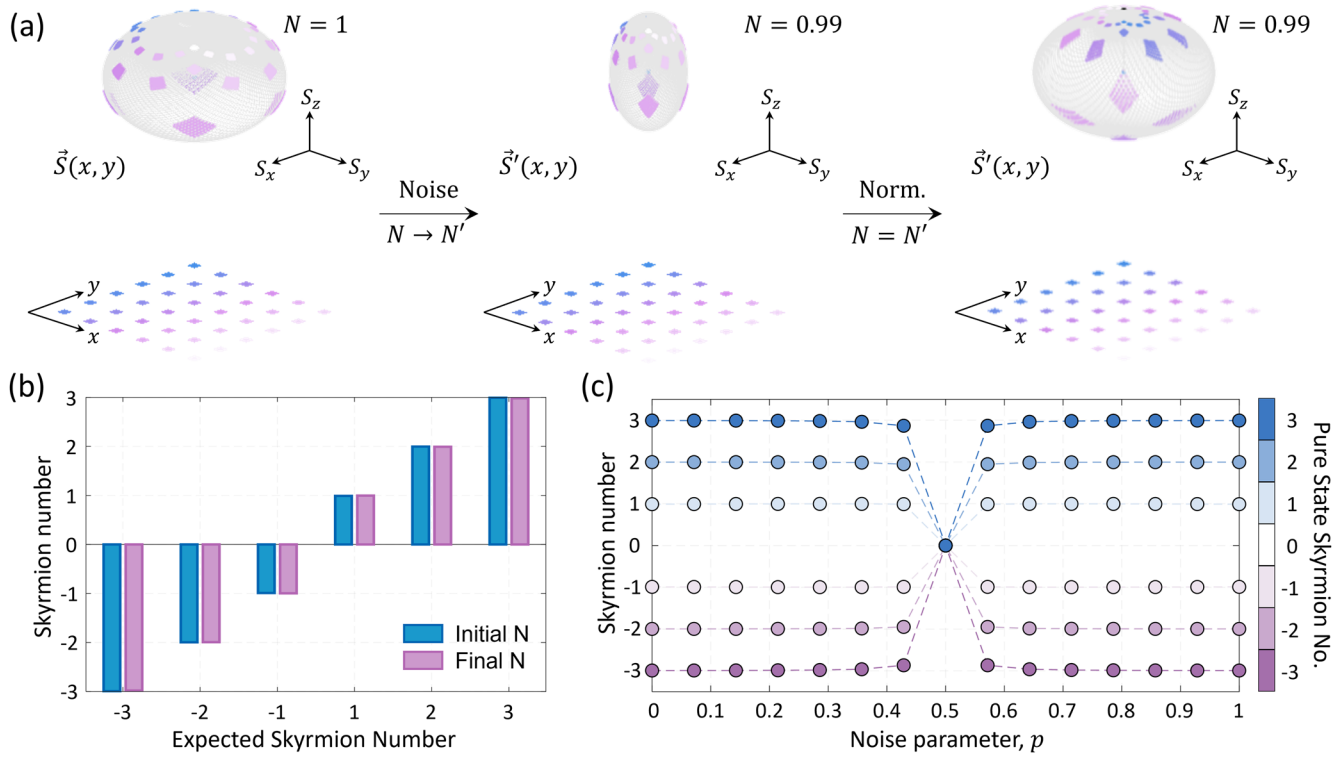


FIG. 7. Skyrmion resilience against constant phase flip channels. (a) Skyrmion map for $N = 1$ before (left panel) and after (middle panel) passing through a constant phase flip channel with a noise parameter of $p = 0.35$. The mapping is clearly distorted, $\vec{S}(x,y) \to \vec{S}'(x,y)$. However, after normalizing $\vec{S}'(x,y)$ such that $\vec{S}'(x,y) \cdot \vec{S}'(x,y) = 1$ (right panel), it is evident that the points have merely shifted without altering the wrapping number. The calculated skyrmion number remains close to the original, $N = 0.99$. This is further illustrated by matching colored regions of interest (ROIs) on the plane with corresponding regions on the sphere, highlighting the shifts that can be corrected by coordinate transformation, i.e., $\vec{S}(x,y) \to \vec{S}'(x,y) \to \vec{S}(x',y')$. (b) Numerically calculated skyrmion numbers (before and after passing through a noisy channel with $p = 0.35$) compared to the expected skyrmion numbers for various topologies, $N \in \{-3,-2,-1,1,2,3\}$, showing clear invariance to the phase flip channel. (c) Skyrmion number plotted against the noise parameter p, demonstrating topological invariance across all phase flip noise settings except at $p = 0.5$, where entanglement is completely lost, reducing N to 0.

interference effects between the signal and noise in the non-linear formula (6).

Further numerical results for various skyrmion topologies passed through constant and spatially varying depolarizing channels are shown in Figs. 9 and 10, respectively. In Fig. 9(a), application of the depolarizing channel with parameter $p = 0.35$ to the initial state $\vec{S}(x,y)$, with a skyrmion number $N = 1$, produces the noisy state $\vec{S}'(x,y)$. This modulation reduces $\vec{S}'(x,y) \cdot \vec{S}'(x,y) < 1$, as expected from the uniform scaling of all components by the factor $1 - p$. This results in a reduction of the radius of the original spherical geometry encoded in the skyrmion wave function. After renormalizing the Stokes parameters so that $\vec{S}'(x,y) \cdot \vec{S}'(x,y) = 1$, it is evident that the depolarizing noise does not affect the orientation of the Stokes vectors. Consequently, the skyrmion number is unaltered, $N \approx 0.99$. In Fig. 9(b), numerical results are presented for skyrmion numbers $N \in \{-3,-2,-1,1,2,3\}$ before (initial) and after (final) passing the state through the constant depolarizing channel, demonstrating the invariance of the topology. Figure 9(c) shows how the skyrmion number remains robust across various depolarizing noise settings, with the topology only breaking down at the extreme limit of $p = 1$. At this point, the state is completely mixed, and entanglement is lost, resulting in $N = 0$. In this scenario, $S_x = S_y = S_z = 0$, and the initial topology cannot be recovered. In Fig. 10(a), numerical results illustrate the distortion of $\vec{S}(x,y)$, with a skyrmion number $N = 1$, after passing through a spatially varying depolarizing channel, where the noise parameter $p(x,y)$ is a smooth function of spatial coordinates defined in (74). Despite the apparent significant distortion of the geometry encoded in the noisy wave function, as compared to the original spherical structure, the skyrmion number remains intact at $N \approx 0.99$. This is again not surprising, as the noise varies smoothly. Figure 10(b) presents results for different topological numbers passed through the same spatially varying noise channel, confirming the robustness of skyrmion topologies against depolarizing noise at various noise levels and with spatially varying noise.

19 May 2025 14:12:42

© Author(s) 2025

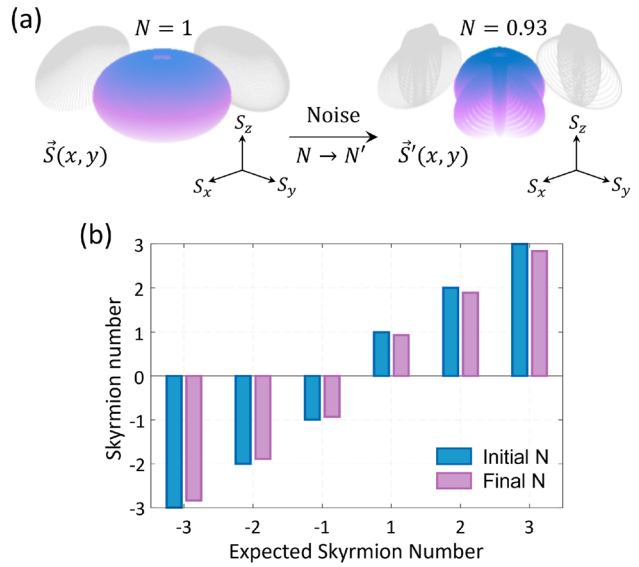


FIG. 8. Skyrmion resilience against a spatially varying phase flip channel. (a) Skyrmion map for $N = 1$ before (left panel) and after (right panel) passing through a spatially varying phase flip channel. Although the mapping is significantly distorted, $\vec{S}(x,y) \to \vec{S}'(x,y)$, the calculated skyrmion number remains close to the expected value, with $N \approx 0.93$. This suggests that despite the heavy distortion, the topological structure is largely preserved. (b) Numerically calculated skyrmion numbers before and after passing through the noisy channel are compared to the expected values for various topologies, $N \in \{-3,-2,-1,1,2,3\}$. The results demonstrate a clear invariance of the topological number, confirming the robustness of the skyrmion topology to spatially varying phase flip noise.

D. Amplitude damping channel

The amplitude damping channel is described by the operators

$$E_0 = \begin{pmatrix} 1 & 0 \\ 0 & \sqrt{1-p} \end{pmatrix}, \qquad E_1 = \begin{pmatrix} 0 & \sqrt{p} \\ 0 & 0 \end{pmatrix}, \tag{75}$$

which obey $E_0^\dagger E_0 + E_1^\dagger E_1 = \mathbf{1}$ with $\mathbf{1}$ the 2×2 identity matrix, and again we must allow p to be a smooth function of x and y. Using this channel, the noisy density matrix is given by

$$\hat{\rho} = \begin{pmatrix} \rho_{11} + p\rho_{22} & \sqrt{1-p}\rho_{12} \\ \sqrt{1-p}\rho_{21} & (1-p)\rho_{22} \end{pmatrix}. \tag{76}$$

The form of the channel parameter p assumed in the numerical analysis is

$$p = (\alpha + \beta \cos(n\phi)) \exp\left(-\gamma\rho^2\right). \tag{77}$$

When $p = 0$, this channel acts as the identity. Notice that as $\rho \to \infty$, $p \to 0$ with the falloff controlled by the parameter γ. We choose $\beta < \alpha$ to ensure that p remains positive. The integer n controls how p oscillates for fixed ρ as ϕ is varied. Our numerical results confirm that the skyrmion number is completely robust to amplitude damping.

For the amplitude damping channel, the Stokes parameters with a constant p are given by

$$\begin{aligned} S_x &= \sqrt{1-p}\, 2^{\frac{|l_1|+|l_2|}{2}} \rho^{|l_1|+|l_2|} w_0^{-|l_1|-|l_2|-2} \\ &\quad \times \frac{\left(1 + e^{2i\phi(l_1-l_2)}\right) e^{-\frac{2\rho^2}{w_0^2} - i\phi(l_1-l_2)}}{\pi\sqrt{|l_1|!|l_2|!}}, \\ S_y &= i\sqrt{1-p}\, 2^{\frac{|l_1|+|l_2|}{2}} \rho^{|l_1|+|l_2|} w_0^{-|l_1|-|l_2|-2} \\ &\quad \times \frac{\left(-1 + e^{2i\phi(l_1-l_2)}\right) e^{-\frac{2\rho^2}{w_0^2} - i\phi(l_1-l_2)}}{\pi\sqrt{|l_1|!|l_2|!}}, \\ S_z &= \left((2p-1)2^{|l_2|}|l_1|!w_0^{2|l_1|}\rho^{2|l_2|} + 2^{|l_1|}|l_2|!\rho^{2|l_1|}w_0^{2|l_2|}\right) \\ &\quad \times \frac{e^{-\frac{2\rho^2}{w_0^2}} w_0^{-2(|l_1|+|l_2|+1)}}{\pi|l_1|!|l_2|!}. \end{aligned} \tag{78}$$

Notice that at $p = 1$, both $S_x = 0$ and $S_y = 0$. The skyrmion number vanishes at this value. The discussion is again parallel to the bit flip and phase flip channels: even though the reparametrization we use for p does pass through $p = \frac{1}{2}$ and $p = 1$ values, the skyrmion number is robust to the amplitude damping channel, and we do not expect these particular channel parameter values to play any role in practice.

Further numerical results for various skyrmion topologies resulting after the state is passed through both constant and spatially varying amplitude damping channels are shown in Figs. 11 and 12, respectively. In Fig. 11(a), the initial map $\vec{S}(x,y)$ with skyrmion number $N = 1$ is transformed into $\vec{S}'(x,y)$ after passing the density matrix through an amplitude damping channel with $p = 0.35$. This produces a geometric distortion of the sphere encoded by the state, with points shifted toward the North Pole while maintaining $\vec{S}'(x,y) \cdot \vec{S}'(x,y) \leq 1$. This behavior is expected since the components of the map transform as follows: $S_x' = S_x\sqrt{1-p}$, $S_y' = S_y\sqrt{1-p}$, and $S_z' = p + S_z(1-p)$, indicating that the x, y components are scaled and S_z is shifted by a positive constant. At $p = 1$, all points collapse to the North Pole, i.e., $\vec{S}'(x,y) = [0,0,1]^T$. After renormalizing the Stokes parameters, it is evident that noise does not affect the Stokes vectors' orientation, so the skyrmion number is unchanged at $N \approx 0.99$. A subtle point should be noted here. Unlike other noise channels studied in this work, amplitude damping channels yield a shift of the Stokes vectors, which may induce numerical errors when normalizing the field; therefore, this is corrected for before normalizing and calculating the skyrmion number. More details are provided in the Appendix. In Fig. 11(b), the numerical results show skyrmion numbers for various topologies $N \in \{-3,-2,-1,1,2,3\}$ before and after passing through the constant amplitude damping channel, establishing the topological robustness. Figure 11(c) displays skyrmion numbers across different amplitude damping noise levels, revealing that the topology is unaffected by noise except at the extreme limit where $p = 1$. At

19 May 2025 14:12:42

© Author(s) 2025

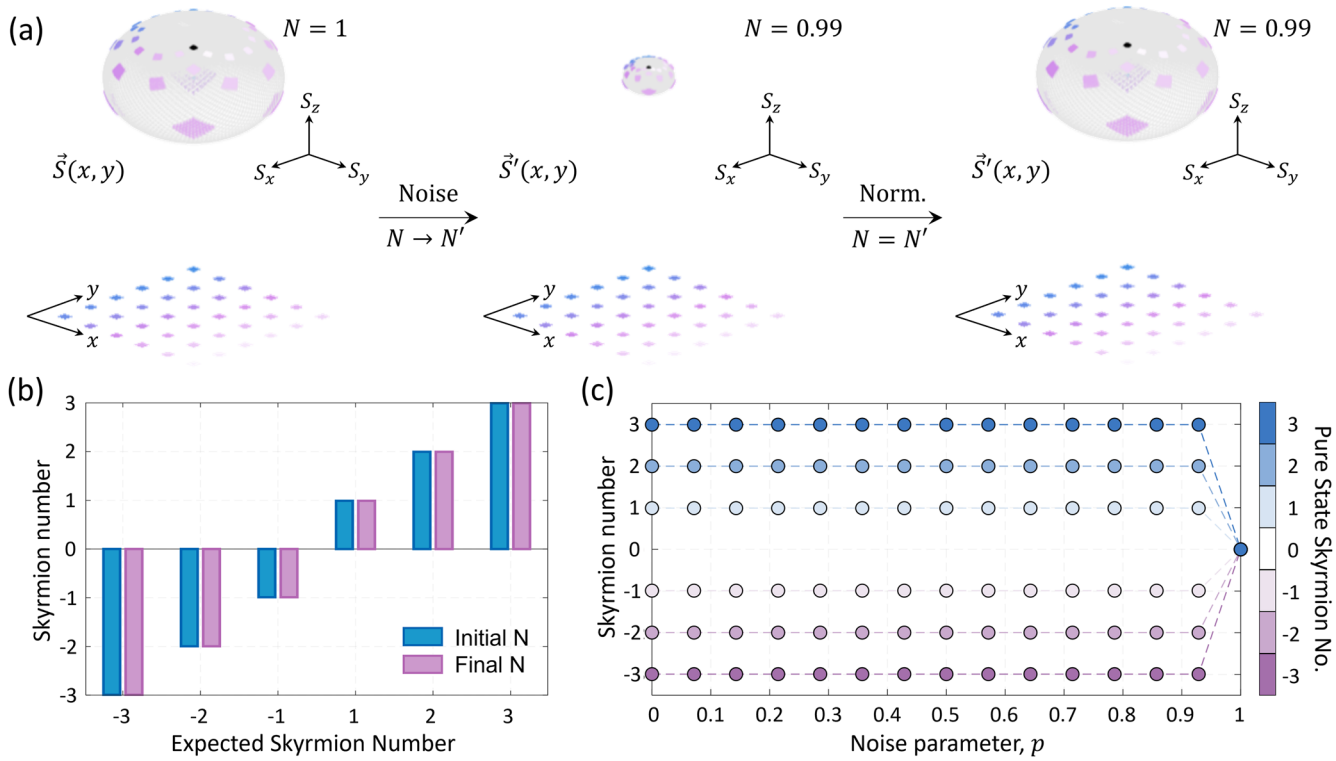


FIG. 9. Skyrmion resilience against constant depolarizing channel. (a) Skyrmion map defined by the density matrix for $N = 1$ before (left panel) and after (middle panel) passing through a constant depolarizing channel with a noise parameter $p = 0.35$. The mapping $\vec{S}(x,y) \to \vec{S}'(x,y)$ shows that the density matrix has suffered a clear distortion due to depolarizing noise, which reduces the magnitude of $\vec{S}(x,y)$, i.e., $\vec{S}(x,y) \cdot \vec{S}(x,y) < 1$. After renormalizing $\vec{S}'(x,y)$ such that $\vec{S}'(x,y) \cdot \vec{S}'(x,y) = 1$ (right panel), the Stokes vectors recover their spherical orientation, and the skyrmion number remains unchanged at $N \approx 0.99$. (b) Numerically calculated skyrmion numbers (before and after passing the wave function through the noisy channel with $p = 0.35$) compared to expected skyrmion numbers for various topologies, $N \in \{-3, -2, -1, 1, 2, 3\}$, demonstrate the topology's invariance to depolarizing noise. (c) The calculated skyrmion number as a function of the noise parameter p shows the robustness of the topology across all depolarizing noise levels, except at $p = 1$, where the state becomes completely mixed and entanglement is lost, which reduces the skyrmion number to $N = 0$.

this point, the state is completely mixed and loses all entanglement, which reduces the skyrmion number to $N = 0$. Intuitively, at $p = 1$, $S_x = S_y = S_z = 0$, and the initial topology cannot be recovered. In Fig. 12(a), numerical results are shown for the distortion of $\vec{S}(x,y)$ with skyrmion number $N = 1$ induced by passing the density matrix through a spatially varying amplitude damping channel with a spatially dependent noise parameter $p(x,y)$, defined according to (74). Despite significant geometric distortion compared to the initial spherical geometry, the skyrmion number remains $N \approx 0.99$. This is a consequence of the fact that the noise parameter is a smooth function of the spatial coordinates. In Fig. 12(b), results for various topologies are shown, demonstrating complete robustness of the skyrmion topology to amplitude damping noise at different noise levels and with spatial variation. These results confirm the invariance of skyrmion topology against amplitude damping noise across a range of conditions.

E. Phase damping channel

The phase damping channel is described by the operators

$$E_0 = \begin{pmatrix} 1 & 0 \\ 0 & \sqrt{1-p} \end{pmatrix}, \qquad E_1 = \begin{pmatrix} 0 & 0 \\ 0 & \sqrt{p} \end{pmatrix}, \tag{79}$$

which obey $E_0^\dagger E_0 + E_1^\dagger E_1 = \mathbf{1}$ with $\mathbf{1}$ the 2×2 identity matrix and again we must allow p to be a smooth function of x and y. The form of the channel parameter assumed for the numerical analysis is

$$p = (\alpha + \beta \cos(n\phi)) \exp\left(-\gamma \rho^2\right), \tag{80}$$

and we choose parameters so that $p \leq 1$. Notice that when $p = 0$, this channel acts as the identity. This channel again acts

19 May 2025 14:12:42

© Author(s) 2025

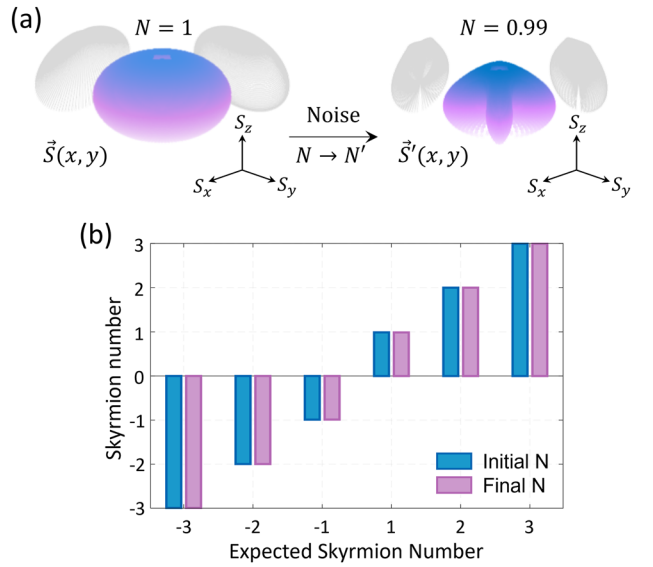


FIG. 10. Skyrmion resilience against a spatially varying depolarizing channel. (a) Skyrmion map for $N = 1$ before (left panel) and after (right panel) passing the density matrix through a spatially varying depolarizing channel. Despite significant distortion in the mapping, $\vec{S}(x,y) \to \vec{S}'(x,y)$, the calculated skyrmion number remains robust, with a value of $N \approx 0.99$, close to the expected value. (b) Numerically calculated skyrmion number, both before and after the state passes through the noisy channel, plotted against the expected skyrmion number for various topologies, $N \in \{-3,-2,-1,1,2,3\}$. The results demonstrate a clear invariance of topology, even under the influence of the spatially varying depolarizing channel.

non-trivially only in a local region centered on $\rho = 0$, with the falloff of p controlled by γ. Our numerical results demonstrate that the skyrmion number is completely robust to the phase damping channel. Specializing to p constant, we find the Stokes parameters

$$
\begin{aligned}
S_x &= \sqrt{1-p}\, 2^{\frac{|l_1|+|l_2|}{2}} \rho^{|l_1|+|l_2|} w_0^{-|l_1|-|l_2|-2} \\
&\quad \times \frac{\left(1+e^{2i\phi(l_1-l_2)}\right) e^{-\frac{2\rho^2}{w_0^2}-i\phi(l_1-l_2)}}{\pi\sqrt{|l_1|!|l_2|!}}, \\
S_y &= i\sqrt{1-p}\, 2^{\frac{|l_1|+|l_2|}{2}} \rho^{|l_1|+|l_2|} w_0^{-|l_1|-|l_2|-2} \\
&\quad \times \frac{\left(e^{2i\phi(l_1-l_2)}-1\right) e^{-\frac{2\rho^2}{w_0^2}-i\phi(l_1-l_2)}}{\pi\sqrt{|l_1|!|l_2|!}}, \\
S_z &= \left(2^{|l_1|}|l_2|!\rho^{2|l_1|} w_0^{2|l_2|} - 2^{|l_2|}|l_1|! w_0^{2|l_1|}\rho^{2|l_2|}\right) \\
&\quad \times \frac{e^{-\frac{2\rho^2}{w_0^2}} w_0^{-2(|l_1|+|l_2|+1)}}{\pi|l_1|!|l_2|!}.
\end{aligned}
\tag{81}
$$

For $p = 1$, S_x and S_y vanish so that the skyrmion number is zero. Once again, we do not expect this particular channel parameter value to play any role in practice.

Numerical results for various skyrmion topologies computed after the density matrix is passed through constant and spatially varying phase damping channels are presented in Figs. 13 and 14, respectively. In Fig. 13(a), the initial skyrmion map $\vec{S}(x,y)$ with skyrmion number $N = 1$ is transformed into $\vec{S}'(x,y)$ by a phase damping channel with noise parameter $p = 0.35$. There is a noticeable distortion of the spherical geometry described by $\vec{S}(x,y)$. This is expected since the S_x and S_y components are scaled by a factor $\sqrt{1-p}$, much like what occurred in the phase flip channel. After renormalizing the Stokes parameters, it is evident that the noise only produces a rotation of the Stokes vectors, as illustrated by the shift in the positions of regions of interest (ROIs) on the sphere. Therefore, the transformation does not alter the skyrmion number, which is $N \approx 0.99$. In Fig. 13(b), numerical results for states with skyrmion numbers $N \in \{-3,-2,-1,1,2,3\}$ are shown before and after the action of the same phase damping channel. In Fig. 13(c), results for these states across different phase damping noise levels are displayed. These results confirm that the skyrmion topology is invariant under phase damping noise, collapsing only at the singular limit $p = 1$, where entanglement is lost and the skyrmion number vanishes. At $p = 1$, $S_x = S_y = 0$, so it is not possible to recover the initial topology. Figure 14(a) shows numerical results for the distortion of $\vec{S}(x,y)$ with skyrmion number $N = 1$ induced by a spatially varying phase damping channel with a spatially dependent noise parameter, $p(x,y)$, as defined in Eq. (68). Although the new map $\vec{S}'(x,y)$ reflects a highly distorted geometry when compared to the initial spherical geometry, the skyrmion number remains robust at $N \approx 0.98$. This is expected since the noise parameter varies smoothly with the spatial coordinates. In Fig. 14(b), the results for various states with a range of topological numbers, all acted on by the same spatially varying phase damping channel, demonstrate the complete robustness of the skyrmion topology under the influence of this type of noise, regardless of noise levels or spatial variation.

VIII. GLOBAL EFFECTS

In Secs. I–VII, we have developed a description for noise that affects only local features of the wave function. Under these conditions it is reasonable to expect that noise leaves the topology intact. However, as we will now explain, certain local noise effects can disturb the topology of the wave function. To understand how this can happen, recall that the integer skyrmion number is the winding number of a map from S^2 to S^2. One of these spheres represents the space of polarization states, while the other is obtained by compactifying the plane $\mathbb{R}^2$ to a sphere. This compactification is achieved by identifying the points at infinity[62] with the North Pole of an S^2. Compactification is only possible if the wave function takes the same value for all points at infinity, as it is only in this case that it makes sense to identify this collection of points with a single point, the North Pole of a sphere. If the compactification condition is not satisfied, the skyrmion number need not even be an integer, and our scheme for the discretization of entanglement fails.

We will discuss this effect in the simplest possible setting. Our skyrmion wave functions lead to Stokes parameters of the following generic form:

19 May 2025 14:12:42

© Author(s) 2025

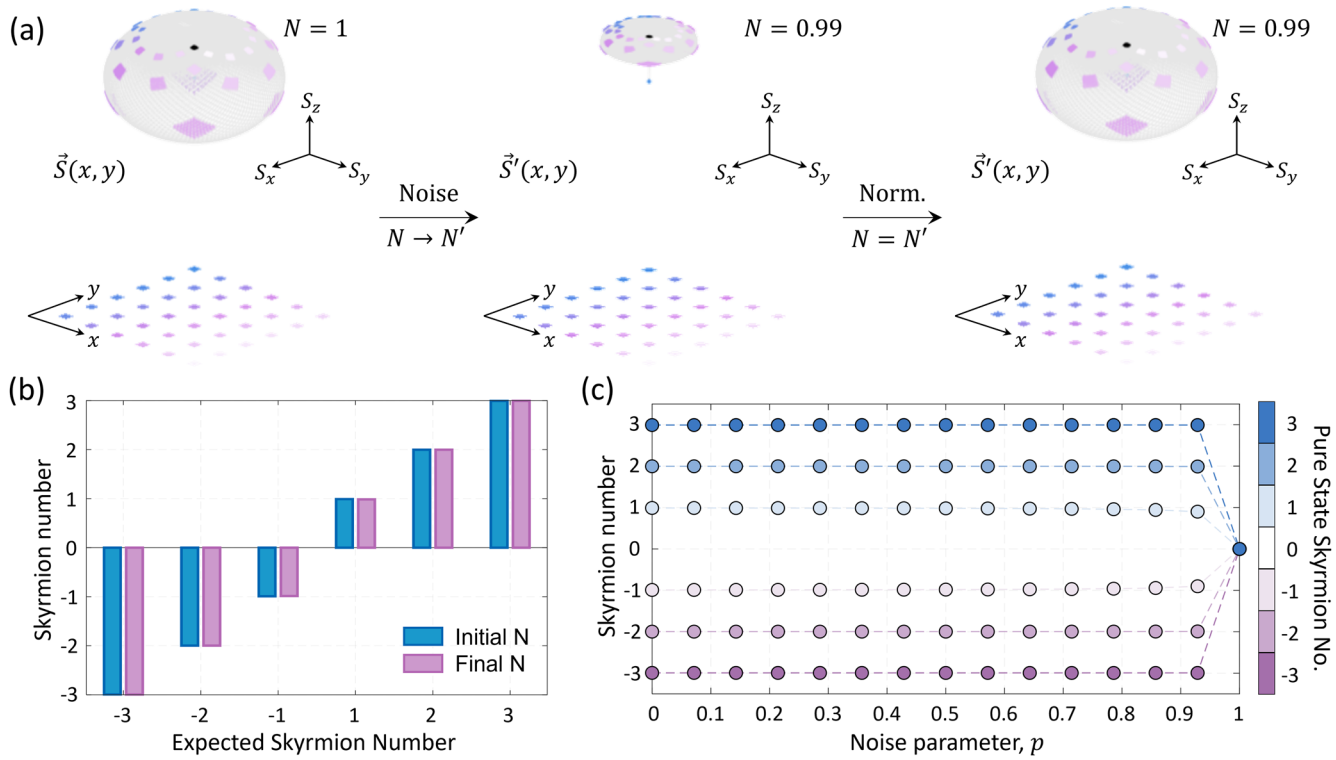


FIG. 11. Skyrmion resilience against constant amplitude damping channel. (a) Skyrmion map for $N = 1$ before (left panel) and after (middle panel) passing the density matrix through a constant amplitude damping channel with a noise parameter of $p = 0.35$. The mapping $\vec{S}(x, y) \to \vec{S}'(x, y)$ shows clear distortion. To properly evaluate the skyrmion number, the map is renormalized (right panel) so that $\vec{S}'(x, y) \cdot \vec{S}'(x, y) = 1$. Despite the distortion, the wrapping number is preserved, with a calculated skyrmion number of $N \approx 0.99$. Matching colors highlight correlated regions of interest on the plane and sphere, exhibiting the movement of points on the sphere. This can be corrected for with a coordinate transformation as $\vec{S}(x, y) \to \vec{S}'(x, y) \to \vec{S}(x', y')$. (b) Numerically calculated skyrmion numbers before and after passing the density matrix through the noisy channel with $p = 0.35$, plotted against the expected skyrmion number for various topologies, $N \in \{-3, -2, -1, 1, 2, 3\}$. This demonstrates that the skyrmion number is robust to noise from the amplitude damping channel. (c) The skyrmion number plotted against the noise parameter, p, demonstrates topological invariance across all noise settings except at $p = 1$, where state entanglement is completely lost and the skyrmion number vanishes.

$$S_x = \frac{2\sqrt{\rho}\sin(k\phi)}{\rho+1}, \quad S_y = \frac{2\sqrt{\rho}\cos(k\phi)}{\rho+1}, \quad S_z = \frac{\rho-1}{\rho+1}. \tag{82}$$

This particular solution has a skyrmion number of k. We now present an argument that, we claim, holds generally for the Stokes parameters under consideration but that uses the particular solution discussed earlier. The justification for applying the specific formula (82) while arriving at a general conclusion lies in the topological nature of the problem. By employing topological methods, we partition the complete set of functions into distinct equivalence classes, where any two functions within the same class can be smoothly deformed into one another. Each equivalence class is characterized by a topological invariant, which in our case is the skyrmion number. Consequently, when making a topological argument about a function (which includes evaluating its skyrmion number), it suffices to consider any representative from its equivalence class. A particularly useful feature of the class of functions identified in (82) is that as k varies over the integers, it spans the entire set of equivalence classes, and solutions with different values of k belong to different topological classes.

The important features of the Stokes parameters (82) are as follows:

1. S_x and S_y are responsible for all of the ϕ dependence.
2. The Stokes vector is normalized to 1: $\vec{S} \cdot \vec{S} = 1$.
3. S_z is -1 at the origin $\rho = 0$, and it tends to 1 as $\rho \to \infty$.

These general features are all that are needed to discuss the compactification condition, and they are all shared with the actual skyrmion solutions we have considered. After a suitable smooth deformation, all sensible skyrmion solutions must have these properties. The key observation is that any solution that enjoys these three properties will obey the compactification condition. Indeed, property 3 above tells us that $S_z = 1$ for the points at infinity, while property 2 then implies that $S_x = 0 = S_y$ for these points. Finally, property 1 then establishes that there is no ϕ dependence in the

19 May 2025 14:12:42

© Author(s) 2025

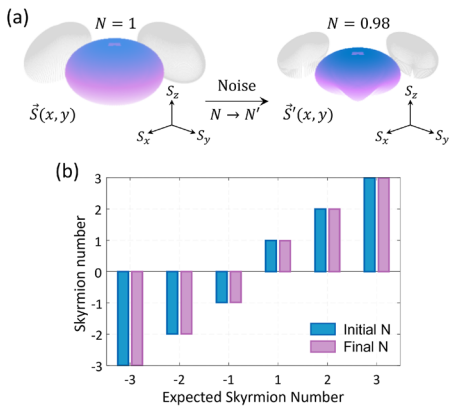


FIG. 12. Skyrmion resilience against a spatially varying amplitude damping channel. (a) Skyrmion map for $N = 1$ before (left panel) and after (right panel) passing the density matrix through a spatially varying amplitude damping channel. Despite significant distortion in the mapping, $\vec{S}(x,y) \to \vec{S}'(x,y)$, the calculated skyrmion number remains essentially unchanged at $N \approx 0.98$. (b) Numerically calculated skyrmion numbers before and after passing the density matrix through the noisy channel are compared against expected values for various skyrmion topologies, $N \in \{-3,-2,-1,1,2,3\}$. The results demonstrate clear topological invariance of the skyrmion number under the spatially varying amplitude damping channel.

Stokes parameters as $\rho \to \infty$ so that we can indeed compactify the plane to S^2. This provides a clean diagnostic of whether or not our solution respects the compactification condition: we simply test if the above-mentioned three conditions hold.

It may sound implausible that noise can affect the behavior of the wave function at infinity. However, a key insight of Ref. 40 is that in practice we never work with the entire plane, but rather with some open subset $U \subset \mathbb{R}^2$. The compactification condition then amounts to the requirement that on the boundary of the open subset U, the Stokes parameters no longer have any ϕ dependence. Noise can disrupt this property by introducing additional ϕ dependence. In this case, the plane cannot be compactified to an S^2, we lose the interpretation of the skyrmion wave functions as a map from S^2 to S^2, and generally, there is no reason to expect that the skyrmion number computed using (6) will give an integer.

We can also examine a scenario where both conditions **2** and **3** are violated in a practical setting, as illustrated in Fig. 15. In this case, depolarizing noise reaches its maximum value, $p = 1$, at a finite radius, $r = a$, as shown in Fig. 15(a). This situation can occur when the signal-to-noise ratio at the periphery becomes too low to detect any meaningful signal, making the state appear maximally mixed, in which case we cannot distinguish the vector of Stokes parameters from the null vector. Within the region where $r < a$, we can maintain $\vec{S}' \cdot \vec{S}' = 1$ after normalization. However, outside this region, for

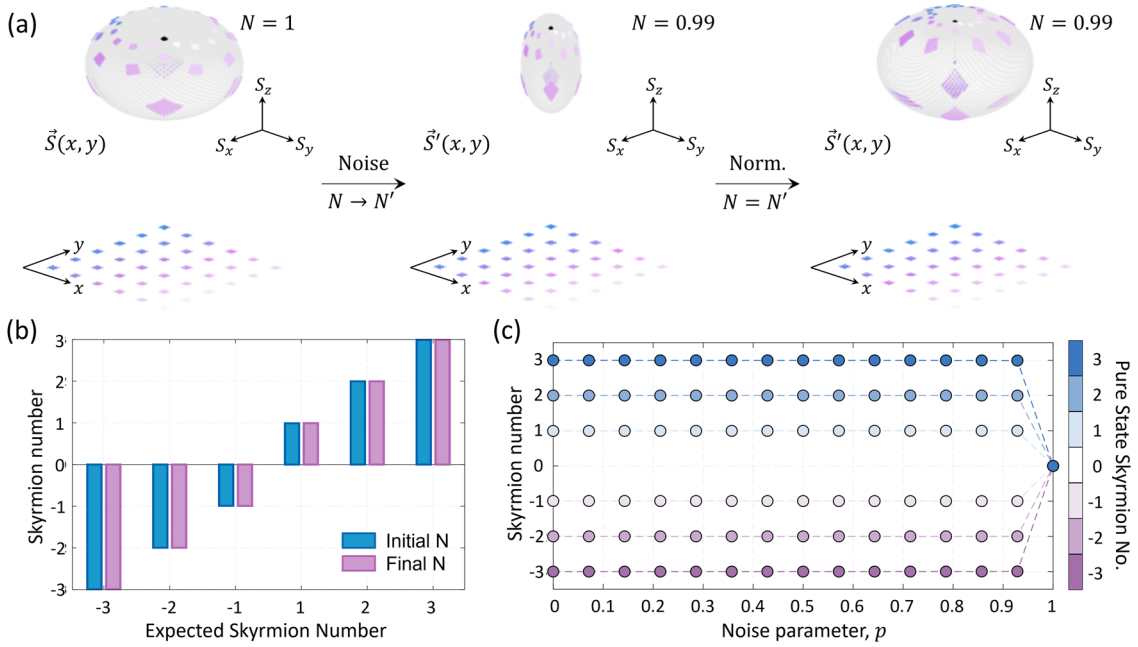


FIG. 13. Skyrmion resilience against constant phase damping channel. (a) Skyrmion map for $N = 1$ before (left panel) and after (middle panel) passing the density matrix through a constant phase damping channel with noise parameter $p = 0.35$. The mapping is visibly distorted, with $\vec{S}(x,y) \to \vec{S}'(x,y)$. Despite the distortion, the skyrmion number, when evaluated for the normalized but distorted map, remains nearly unchanged, $N = 0.99$. This is explained by noting that points on the sphere have merely shifted, as can be seen from the correlated regions of interest (highlighted in matching colors). These shifts on the sphere can be corrected by a coordinate transformation acting on the plane, i.e., $\vec{S}(x,y) \to \vec{S}'(x,y) \to \vec{S}(x',y')$. (b) Numerically calculated skyrmion numbers before and after application of the noisy channel (with $p = 0.35$) compared to the expected skyrmion numbers for various topologies $N \in \{-3,-2,-1,1,2,3\}$. This establishes the invariance of the skyrmion number to the effects of phase damping noise. (c) The skyrmion number is plotted against the noise parameter p, demonstrating the robustness of the skyrmion topology across all phase damping noise parameter values, except at $p = 1$, where entanglement is completely lost.

19 May 2025 14:12:42

© Author(s) 2025

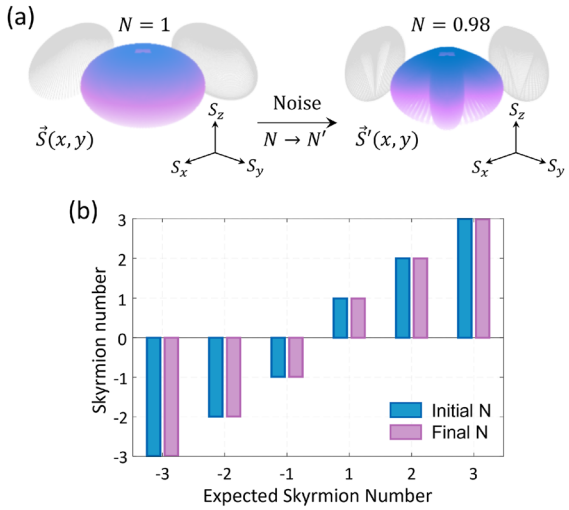


FIG. 14. Skyrmion resilience against a spatially varying phase damping channel. (a) Skyrmion map for $N = 1$ before (left panel) and after (right panel) the effects of noise due to a spatially varying phase damping channel are included. Despite the significant distortion of the map, $\vec{S}(x,y) \to \vec{S}'(x,y)$, the calculated skyrmion number remains close to the expected value at $N \approx 0.98$. (b) Numerically calculated skyrmion numbers, before and after the action of the noisy channel, are compared for various topologies, $N \in \{-3,-2,-1,1,2,3\}$. The results demonstrate a clear invariance of the skyrmion topology to the spatially varying phase damping channel.

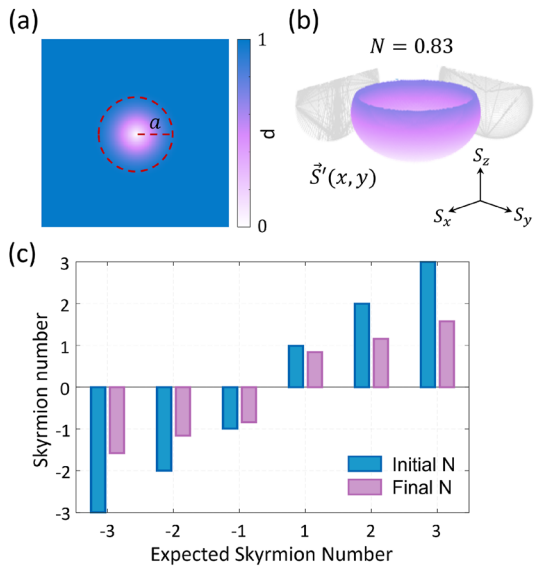


FIG. 15. Violation of the skyrmion compactification condition. (a) A spatially varying depolarizing noise function where $p < 1$ inside the outlined region (dashed red circle) and $p = 1$ outside of it. (b) The noisy skyrmion map, $\vec{S}'(x,y)$, for $N = 1$ after normalization, showing partial coverage of the Poincaré sphere, with a calculated skyrmion number of $N \approx 0.83$. (c) Numerically calculated skyrmion numbers before and after passing through the noisy channel for various topologies, $N \in \{-3,-2,-1,1,2,3\}$, demonstrating the loss of integer discretization in the topological signal.

$r \geq a$, this condition can no longer be satisfied, as $\vec{S}' \cdot \vec{S}' = 0$. This breakdown is also depicted in Fig. 15(b), which shows a clear loss of coverage of the Poincaré sphere by the map $\vec{S}'$. Such violations generally lead to maps with non-integer skyrmion numbers, as further illustrated in Fig. 15(c), where states with different topologies are passed through the same channel.

IX. CONCLUSIONS

In this paper, we have examined a scheme that discretizes bipartite entanglement by leveraging the non-trivial topology of the two photon entangled wave function. Our primary focus has been to investigate the robustness of the resulting discrete signal against noise.

Discrete signals are inherently robust against noise because the noise must induce a transition between discrete values before any effects are observed. Moreover, since topology is encoded into the global features of the wave function, noise that only induces local changes is unlikely to disturb the topology. Intuitively, transitions between discrete values are not easily affected by noise, allowing our scheme to benefit from a natural topological noise rejection property.

For non-depolarizing sources of noise, our description employs a quantum channel with a single Kraus operator. In this scenario, we constructed a rigorous argument based on homotopies between the noisy and noise-free density matrices, which establishes the topological noise rejection property. This theoretical argument was corroborated by explicit numerical analyses.

Quantum channels that describe depolarizing noise inherently involve a sum over Kraus operators, rendering a homotopy analysis inapplicable. The basic point is that each term in the Kraus operator sum contributes to the Stokes parameters, and since the skyrmion number (6) is cubic in the Stokes parameters, there will be interference effects between the contributions from different channels. Arguing that homotopies exist for the individual channel terms does not constrain their interference so that the existence of homotopies no longer implies the invariance of the skyrmion number. Nevertheless, numerical analysis can still be performed. Our findings confirm that the skyrmion number remains robust even under the influence of depolarizing noise.

Finally, the integer skyrmion number is the winding number of a map from S^2 to S^2. The base sphere is obtained by compactifying the plane $\mathbb{R}^2$, and the target sphere is the space of polarization states. Compactification of the plane identifies the points at infinity (points with $\rho = \infty$ and any ϕ) as a single point. This is only possible if the wave function becomes independent of ϕ as $\rho \to \infty$. If the wave function fails to meet this condition, the invariant computed using (6) can no longer be considered a skyrmion number and is not generically an integer: the discretization of entanglement through the use of topology fails.

The results of this paper establish the conditions under which the skyrmion topology is robust to the influence of noise. While our study focused on the skyrmion topology derived from the entanglement of spatially separated photons, it can readily be applied to classical non-separable vector states[63,64] and single photon spin–orbit coupled states.[65,66] The advantage of studying non-local states is that they offer extra noise mitigation strategies that involve the

19 May 2025 14:12:42

© Author(s) 2025

exploitation of the ability to spatially separate the DoFs in a given noisy quantum channel. In channels where the topology may indeed undergo transitions, non-local states may offer strategies to circumvent the loss of topology by altering how the photons are passed through the channel. Our model for the noise is novel, and we believe it gives a solid foundation for further investigations into the topological resilience of carefully defined entanglement observables. We hope our findings will motivate further developments in this exciting field.

ACKNOWLEDGMENTS

This work was supported by the South African National Research Foundation/CSIR Rental Pool Program. The research of RdMK is supported by a start-up research fund from Huzhou University, a Zhejiang Province talent award, and a Changjiang Scholar award. B.-Q.L. is supported by the National Natural Science Foundation of China under Grant No. 12405058 and by the Zhejiang Provincial Natural Science Foundation of China under Grant No. LQ23A050002.

AUTHOR DECLARATIONS

Conflict of Interest

The authors have no conflicts to disclose.

Author Contributions

R.d.M.K. and B.-Q.L. provided the theoretical framework. R.d.M.K., B.-Q.L., and P.O. performed the numerical simulations. All authors contributed to the writing of the paper and analysis of data. The idea for the project was conceived by R.d.M.K., P.O., I.N., and A.F. R.d.M.K. and A.F. supervised the project.

Robert de Mello Koch: Conceptualization (equal); Investigation (equal); Methodology (equal); Writing – original draft (equal); Writing – review & editing (equal). **Bo-Qiang Lu**: Investigation (equal); Writing – original draft (equal); Writing – review & editing (equal). **Pedro Ornelas**: Data curation (equal); Investigation (equal); Writing – original draft (equal); Writing – review & editing (equal). **Isaac Nape**: Conceptualization (equal); Investigation (equal); Methodology (equal); Writing – original draft (equal); Writing – review & editing (equal). **Andrew Forbes**: Conceptualization (equal); Investigation (equal); Supervision (equal); Writing – original draft (equal); Writing – review & editing (equal).

DATA AVAILABILITY

The data that support the findings of this study are available from the corresponding authors upon reasonable request.

APPENDIX: NUMERICAL SIMULATIONS

Here, we present important details concerning the numerical evaluation of the Skyrmion number for hybrid states.

1. Simulation calibration

The skyrmion number for a given state was calculated using (6). This expression involves taking an integral over all of space; therefore, numerically, it is necessary to ensure that the integrand is adequately sampled (high enough resolution) and, furthermore, that the finite domain over which we integrate is large enough, thereby ensuring that we adequately approximate full coverage over the entirety of the Poincaré sphere. To this end, we investigate the behavior of the skyrmion number as the resolution of the field and domain of integration is altered. From this we select adequate simulation parameters for the evaluations undertaken in this work.

a. Resolution simulations

By altering the beam waist, w_0, of the spatial LG modes given in (2) with respect to the pixel size, dx, used in the simulation and monitoring the behavior of the skyrmion number, we can investigate the impact of resolution on the evaluation of the skyrmion number. These simulations are shown in Fig. 16(a), where the skyrmion number is plotted as a function of the beam waist normalized against the pixel size for states with skyrmion numbers $N = \{-3, -2, -1, 0, 1, 2, 3\}$. Clearly, when the ratio, $\frac{w_0}{dx}$, is below 20, the evaluation of the skyrmion number is unreliable; therefore, we have chosen w_0 and dx such that $\frac{w_0}{dx} > 20$. This is further emphasized by the example plots shown for the skyrmion density, Σ_z, for $\frac{w_0}{dx}$ values of 1, 23, and 58, respectively. Rather unsurprisingly, for $\frac{w_0}{dx} \approx 1$, the skyrmion number evaluation fails, returning a value of $N = -0.90$ when $N = 3$ was the expected theoretical value. For $\frac{w_0}{dx} \approx 23$ and $\frac{w_0}{dx} \approx 58$, we calculate values of $N = 2.92$ and $N = 2.99$, respectively. Depending on the desired degree of accuracy, one can further increase $\frac{w_0}{dx}$, which better approximates the continuous nature of the field, at the expense of computational resources.

b. Integration domain simulations

The integration radius, r_0, of the integral given in (6) was altered with respect to the beam waist, and the behavior of the skyrmion number was monitored to investigate the impact of the integration domain on the evaluation of the skyrmion number. These simulations are shown in Fig. 16(b), where the skyrmion number is plotted as a function of the integration radius normalized against the beam waist for states with skyrmion numbers $N = \{-3, -2, -1, 0, 1, 2, 3\}$. Clearly, when the ratio, $\frac{r_0}{w_0}$, is below 3, the evaluation of the skyrmion number is unreliable; therefore, we have chosen r_0 and w_0 such that $\frac{r_0}{w_0} > 3$. This is further emphasized by the example plots shown for the skyrmion field, Σ_z, for $\frac{r_0}{w_0}$ values of 0.5, 2, and 10, respectively. For $\frac{r_0}{w_0} \approx 0.5$, the skyrmion number evaluation fails, returning a value of $N = 0.25$ when $N = 3$ was the expected theoretical value. For $\frac{r_0}{w_0} \approx 2$ and $\frac{r_0}{w_0} \approx 10$, we calculate values of $N = 2.59$ and $N = 2.99$, respectively. Depending on the desired degree of accuracy, one can further increase $\frac{r_0}{w_0}$, which better approximates the full coverage over the sphere, at the expense of computational resources.

c. Simulation parameters used

In the simulations presented in this paper, we have used a pixel resolution of 500×500 with a pixel size, $dx = 8$ μm, and a beam waist of $w_0 = 0.3$ mm. These parameters guarantee accurate

19 May 2025 14:12:42

© Author(s) 2025

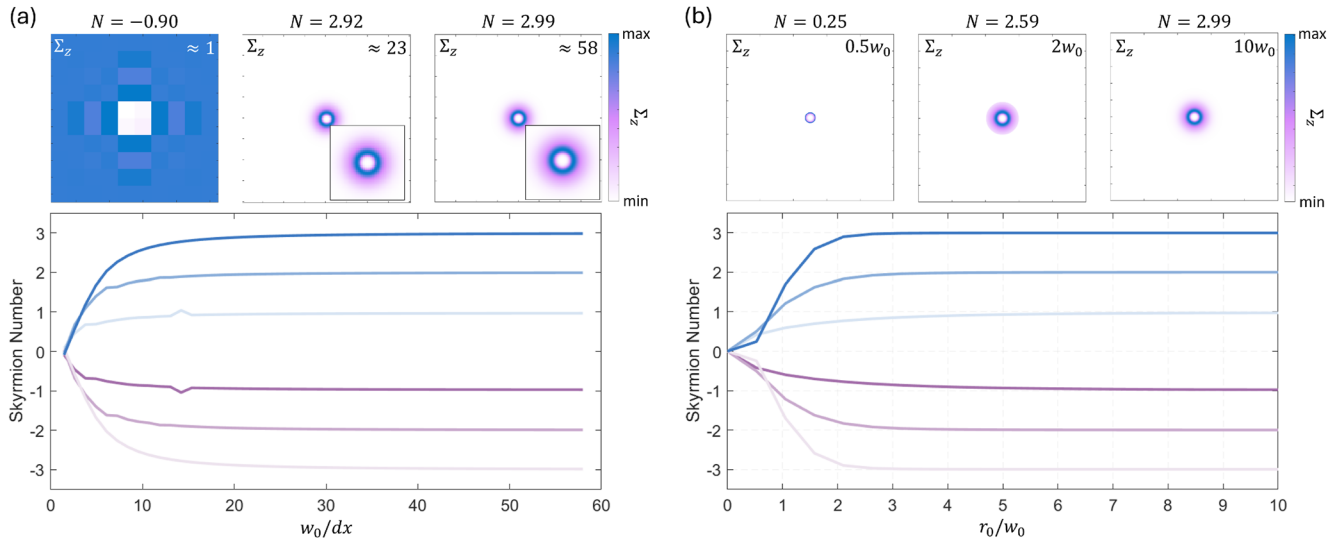


FIG. 16. Resolution and field truncation simulations for skyrmion number calculation. (a) Skyrmion number plotted as a function of the beam waist, w_0, normalized against the pixel size, dx, with some example plots shown for the Skyrme field, Σ_z, for $\frac{w_0}{dx}$ values of 1, 23, and 58, respectively. (b) Skyrmion number plotted as a function of the integration radius, r_0, normalized against the beam size, w_0, with some example plots shown for the Skyrme field, Σ_z, for $\frac{r_0}{w_0}$ values of 0.5, 2, and 10, respectively.

numerical calculations of the skyrmion number, as the values $\frac{w_0}{dx} \approx 38$ and $\frac{r_0}{w_0} \approx 13$ ensure that we are well within the regimes that allow for an accurate numerical evaluation of the skyrmion number. It should be noted that the calibration results presented in Fig. 16 may alter with the use of different fields used to produce the same topological numbers; therefore, it is always necessary to first perform a calibration simulation, which informs the selection of simulation parameters in the experiment. Furthermore, evaluating the skyrmion number through a line integral approach has also been shown to yield advantages when calculating the skyrmion number in noisy environments.[67]

2. Amplitude damping

For most noise scenarios considered in this work, the quantum Stokes parameters derived from a given state either rotate or scale in magnitude after passing through the noise channel, a process that only requires renormalization in order to correctly evaluate the skyrmion number according to (6). However, in addition to scaling, amplitude damping channels also shift the quantum Stokes parameters away from the origin according to $S_x' = S_x\sqrt{1-p}$, $S_y' = S_y\sqrt{1-p}$, and $S_z' = p + S_z(1-p)$, as depicted in Fig. 17(a) (showing the initial "noiseless" state) and (b) (showing the state after passing through an amplitude damping channel) for $p = 0.75$. If the noise is sufficient to shift the map, $\vec{S}'$, such that the origin is no longer contained within the geometric object traced out by $\vec{S}'$, then simply renormalizing the field will collapse the object to a portion of the initial sphere, as shown in Fig. 17(c), from which a skyrmion number $N \approx 0$ is calculated. This occurs because the local normalization performed, $\tilde{\vec{S}}(x,y)' = \frac{\vec{S}'(x,y)}{|\vec{S}'(x,y)|}$, is performed about the origin point, $\vec{O} = (0,0,0)^T$. Such an operation can lead to the premature transition of the topology of the state. Instead, it is first necessary to perform a simple translation operation on the map, thus shifting its center back to the origin, and then performing the normalization, depicted in Figs. 17(d) and 17(e), respectively. Such an operation is perfectly consistent with homotopic arguments presented in this work, as a constant shift over the map cannot alter its topology. Furthermore, no additional prior information is necessary in order to discern the appropriate shift, as it can be discerned from the distorted map, $\vec{S}'$.

3. Stochastic simulations

When considering spatially varying noise functions, $p(x,y)$, we have considered simple analytic functions that describe the noise variation as a function of x, y. However, the homotopic and topological resilience arguments provided within the text do not make use of the functional form of these expressions; they were merely considered out of convenience. More generally, $p(x,y)$ may be chosen as a stochastic spatially varying smooth field where the degree of "randomness" can be directly controlled. To control this degree of randomness, random matrices of size $M \times M$ containing values 0 and 1 were generated, where the size of this matrix relative to the initial simulation matrix of size $N \times N$ ($N = 500$ in this case) dictates the degree of "randomness." We define a controllable parameter, the correlation length, L_c, given as a ratio between w_0 and the random matrix pixel sizes. The lower resolution random matrix is then interpolated (using a bicubic interpolation routine) in order to create a final random smoothly varying noise function, $p(x,y)$. Figure 18 shows simulation results for the illustrative example of states in the presence of isotropic noise with varying randomness and across different random noise iterations shown in Figs. 18(a) and 18(b), respectively, verifying the invariance of topology in the presence of stochastic spatially varying isotropic noise channels.

19 May 2025 14:12:42

© Author(s) 2025

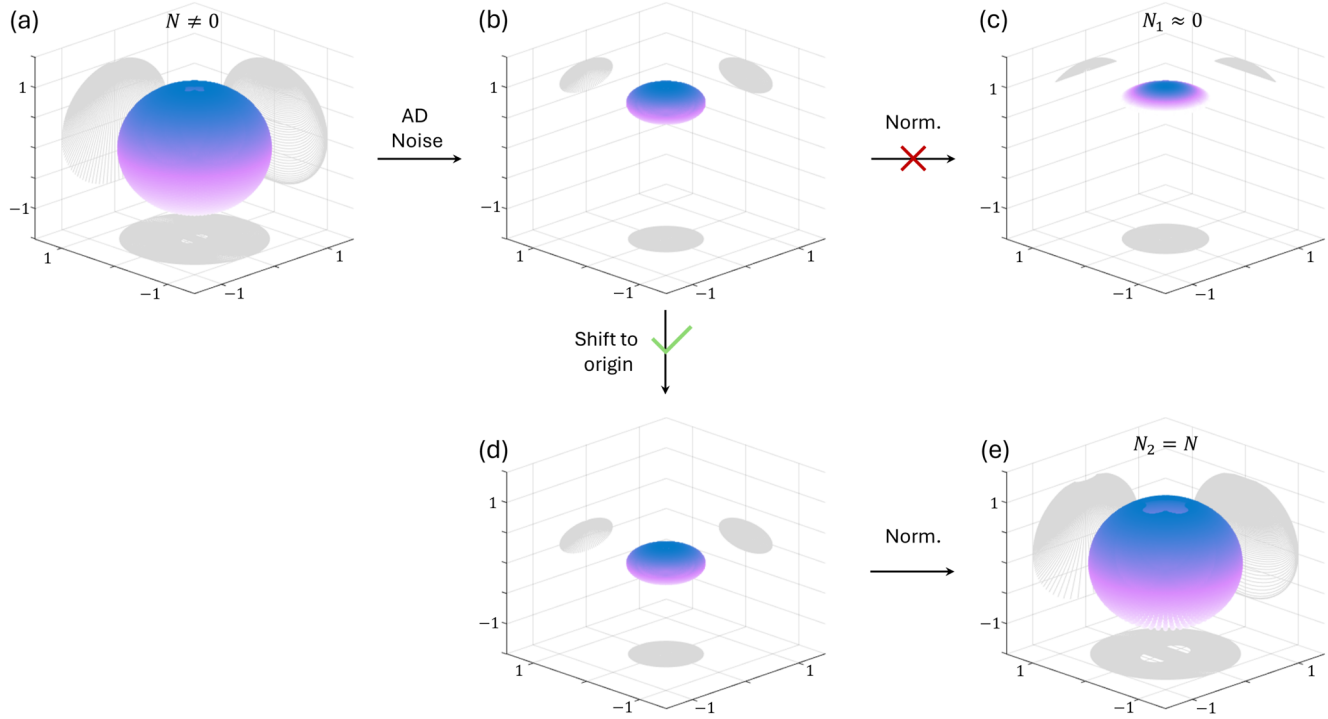


FIG. 17. Numerical considerations for amplitude damping channels. Under the influence of amplitude damping noise, (a) the geometry traced out by the quantum Stokes parameters (which forms a map, $\vec{S} : R^2 \rightarrow S^2$, characterized by the skyrmion number N) (b) shifts above the origin and scales in magnitude. (c) Renormalizing the quantum Stokes parameters at this point yields a false evaluation of the topology, $N_1 \approx 0$, of the state as the normalization is performed about the origin. If instead the (d) map is first shifted back to the origin and then (e) the normalization is performed, this yields a corrected map from which the skyrmion number, $N_2 = N$, can be correctly calculated.

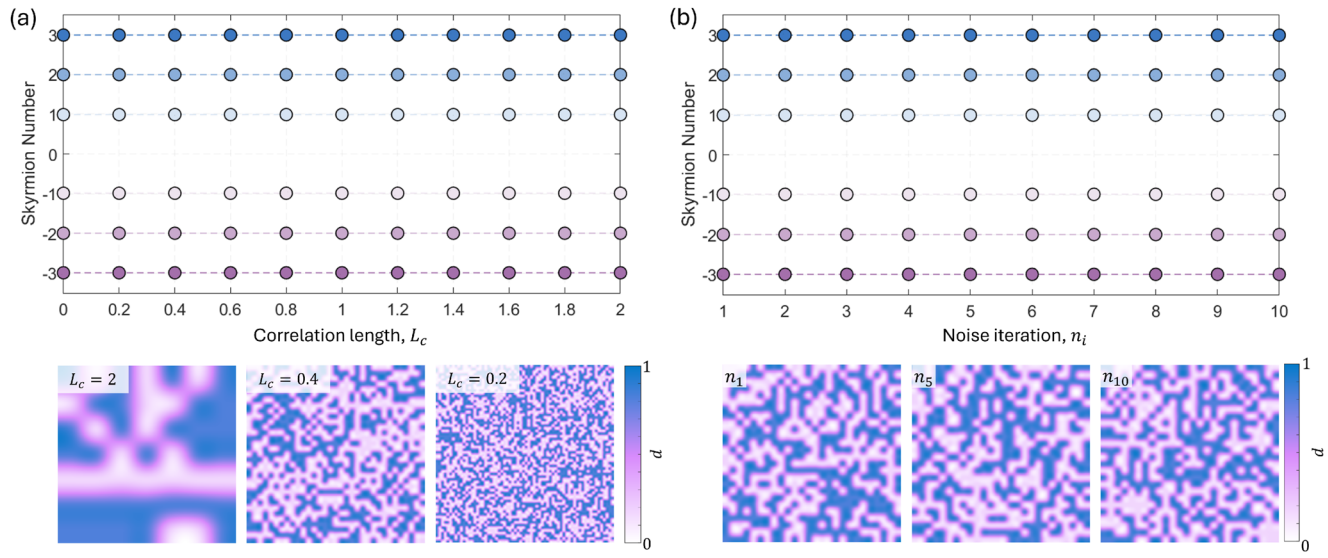


FIG. 18. Stochastic noise simulations. (a) Skyrmion number plotted as a function of the correlation length, L_c, of the random (stochastic) noise functions, $p(x, y)$, for a depolarizing channel with 3 example noise functions of correlation lengths 2, 0.4, and 0.2, shown to illustrate increasing "randomness" with decreasing L_c. (b) Skyrmion number plotted for different iterations of the random noise function $p(x, y)$ with correlation length $L_c = 0.5$, with 3 example iterations of noise functions with $L_c = 0.5$, showing the variation among different random iterations of $p(x, y)$ for the same L_c.

19 May 2025 14:12:42

© Author(s) 2025

REFERENCES

[1]T. Durt, N. J. Cerf, N. Gisin, and M. Żukowski, "Security of quantum key distribution with entangled qutrits," Phys. Rev. A **67**(1), 012311 (2003).

[2]J. Yin, Y.-H. Li, S.-K. Liao, M. Yang, Y. Cao, L. Zhang, J.-G. Ren, W.-Q. Cai, W.-Y. Liu, S.-L. Li *et al.*, "Entanglement-based secure quantum cryptography over 1,120 kilometres," Nature **582**(7813), 501–505 (2020).

[3]F. Basso Basset, M. Valeri, E. Roccia, V. Muredda, D. Poderini, J. Neuwirth, N. Spagnolo, M. B. Rota, G. Carvacho, F. Sciarrino, and R. Trotta, "Quantum key distribution with entangled photons generated on demand by a quantum dot," Sci. Adv. **7**(12), eabe6379 (2021).

[4]C.-H. Liao, C.-W. Yang, and T. Hwang, "Dynamic quantum secret sharing protocol based on GHZ state," Quantum Inf. Process. **13**, 1907–1916 (2014).

[5]M. Hillery, V. Bužek, and A. Berthiaume, "Quantum secret sharing," Phys. Rev. A **59**(3), 1829 (1999).

[6]A. Harrow, P. Hayden, and D. Leung, "Superdense coding of quantum states," Phys. Rev. Lett. **92**(18), 187901 (2004).

[7]J. T. Barreiro, T.-C. Wei, and P. G. Kwiat, "Beating the channel capacity limit for linear photonic superdense coding," Nat. Phys. **4**(4), 282–286 (2008).

[8]J. L. O'brien, "Optical quantum computing," Science **318**(5856), 1567–1570 (2007).

[9]N. Maring, A. Fyrillas, M. Pont, E. Ivanov, P. Stepanov, N. Margaria, W. Hease, A. Pishchagin, A. Lemaître, I. Sagnes *et al.*, "A versatile single-photon-based quantum computing platform," Nat. Photonics **18**(6), 603–609 (2024).

[10]A. Mair, A. Vaziri, G. Weihs, and A. Zeilinger, "Entanglement of the orbital angular momentum states of photons," Nature **412**(6844), 313–316 (2001).

[11]A. Forbes and I. Nape, "Quantum mechanics with patterns of light: Progress in high dimensional and multidimensional entanglement with structured light," AVS Quantum Sci. **1**(1), 011701 (2019).

[12]J. M. Donohue, M. Mastrovich, and K. J. Resch, "Spectrally engineering photonic entanglement with a time lens," Phys. Rev. Lett. **117**(24), 243602 (2016).

[13]J. Brendel, E. Mohler, and W. Martienssen, "Experimental test of Bell's inequality for energy and time," Europhys. Lett. **20**(7), 575 (1992).

[14]J. Brendel, N. Gisin, W. Tittel, and H. Zbinden, "Pulsed energy-time entangled twin-photon source for quantum communication," Phys. Rev. Lett. **82**(12), 2594 (1999).

[15]E. Nagali and F. Sciarrino, "Generation of hybrid polarization-orbital angular momentum entangled states," Opt. Express **18**(17), 18243–18248 (2010).

[16]E. Karimi, J. Leach, S. Slussarenko, B. Piccirillo, L. Marrucci, L. Chen, W. She, S. Franke-Arnold, M. J. Padgett, and E. Santamato, "Spin-orbit hybrid entanglement of photons and quantum contextuality," Phys. Rev. A **82**(2), 022115 (2010).

[17]L. Neves, G. Lima, A. Delgado, and C. Saavedra, "Hybrid photonic entanglement: Realization, characterization, and applications," Phys. Rev. A **80**(4), 042322 (2009).

[18]I. Nape, A. G. de Oliveira, D. Slabbert, N. Bornman, J. Francis, P. H. Souto Ribeiro, and A. Forbes, "An all-digital approach for versatile hybrid entanglement generation," J. Opt. **24**(5), 054003 (2022).

[19]S. P. Walborn, S. Pádua, and C. H. Monken, "Hyperentanglement-assisted Bell-state analysis," Phys. Rev. A **68**(4), 042313 (2003).

[20]W.-B. Gao, C.-Y. Lu, X.-C. Yao, P. Xu, O. Gühne, A. Goebel, Y.-A. Chen, C.-Z. Peng, Z.-B. Chen, and J.-W. Pan, "Experimental demonstration of a hyper-entangled ten-qubit Schrödinger cat state," Nat. Phys. **6**(5), 331–335 (2010).

[21]Z. Xie, T. Zhong, S. Shrestha, X. A. Xu, J. Liang, Y.-X. Gong, J. C. Bienfang, A. Restelli, J. H. Shapiro, F. N. C. Wong, and C. Wei Wong, "Harnessing high-dimensional hyperentanglement through a biphoton frequency comb," Nat. Photonics **9**(8), 536–542 (2015).

[22]F.-G. Deng, B.-C. Ren, and X.-H. Li, "Quantum hyperentanglement and its applications in quantum information processing," Sci. Bull. **62**(1), 46–68 (2017).

[23]D. Kumar and P. N. Pandey, "Effect of noise on quantum teleportation," Phys. Rev. A **68**(1), 012317 (2003).

[24]S. Lloyd, "Capacity of the noisy quantum channel," Phys. Rev. A **55**(3), 1613 (1997).

[25]H.-Q. Liang, J.-M. Liu, S.-S. Feng, and J.-G. Chen, "Quantum teleportation with partially entangled states via noisy channels," Quantum Inf. Process. **12**(8), 2671–2687 (2013).

[26]Q. Yan, X. Hu, Y. Fu, C. Lu, C. Fan, Q. Liu, X. Feng, Q. Sun, and Q. Gong, "Quantum topological photonics," Adv. Opt. Mater. **9**(15), 2001739 (2021).

[27]M. Jalali Mehrabad, A. P. Foster, R. Dost, E. Clarke, P. K. Patil, A. M. Fox, M. S. Skolnick, and L. R. Wilson, "Chiral topological photonics with an embedded quantum emitter," Optica **7**(12), 1690–1696 (2020).

[28]T. Dai, Y. Ao, J. Bao, J. Mao, Y. Chi, Z. Fu, Y. You, X. Chen, C. Zhai, B. Tang *et al.*, "Topologically protected quantum entanglement emitters," Nat. Photonics **16**(3), 248–257 (2022).

[29]S. Mittal, E. A. Goldschmidt, and M. Hafezi, "A topological source of quantum light," Nature **561**(7724), 502–506 (2018).

[30]S. Barik, A. Karasahin, C. Flower, T. Cai, H. Miyake, W. DeGottardi, M. Hafezi, and E. Waks, "A topological quantum optics interface," Science **359**(6376), 666–668 (2018).

[31]A. Blanco-Redondo, B. Bell, D. Oren, B. J. Eggleton, and M. Segev, "Topological protection of biphoton states," Science **362**(6414), 568–571 (2018).

[32]Y. Shen, Q. Zhang, P. Shi, L. Du, X. Yuan, and A. V. Zayats, "Optical skyrmions and other topological quasiparticles of light," Nat. Photonics **18**(1), 15–25 (2024).

[33]Y. Shen, H. Wang, and S. Fan, "Free-space topological optical textures: Tutorial," Adv. Opt. Photonics **17**(2), 295–374 (2025).

[34]T. He, Y. Meng, L. Wang, H. Zhong, N. Mata-Cervera, D. Li, P. Yan, Q. Liu, Y. Shen, and Q. Xiao, "Optical skyrmions from metafibers with subwavelength features," Nat. Commun. **15**(1), 10141 (2024).

[35]Y. Shen, C. He, Z. Song, B. Chen, H. He, Y. Ma, J. A. J. Fells, S. J. Elston, S. M. Morris, M. J. Booth, and A. Forbes, "Topologically controlled multiskyrmions in photonic gradient-index lenses," Phys. Rev. Appl. **21**(2), 024025 (2024).

[36]C. Mitra, C. S. Madasu, L. Gabardos, C. C. Kwong, Y. Shen, J. Ruostekoski, and D. Wilkowski, "Topological optical skyrmion transfer to matter," APL Photonics **10**(4), 046113 (2025).

[37]R. Tamura, S. R. Allam, N. M. Litchinitser, and T. Omatsu, "Three-dimensional projection of optical hopfion textures in a material," ACS Photonics **11**(11), 4958–4965 (2024).

[38]P. Ornelas, I. Nape, R. de Mello Koch, and A. Forbes, "Non-local skyrmions as topologically resilient quantum entangled states of light," Nat. Photonics **18**(3), 258–266 (2024).

[39]J. Chen, A. Forbes, and C.-W. Qiu, "More than just a name? From magnetic to optical skyrmions and the topology of light," Light: Sci. Appl. **14**(1), 28 (2025).

[40]A. A. Wang, Z. Zhao, Y. Ma, Y. Cai, R. Zhang, X. Shang, Y. Zhang, J. Qin, Z.-K. Pong, T. Marozsák, B. Chen, H. He, L. Luo, M. J. Booth, S. J. Elston, S. M. Morris, and C. He, "Topological protection of optical skyrmions through complex media," Light Sci. Appl. **13**, 314 (2024).

[41]C. Liu, S. Zhang, S. A. Maier, and H. Ren, "Disorder-induced topological state transition in the optical skyrmion family," Phys. Rev. Lett. **129**(26), 267401 (2022).

[42]P. Ornelas, I. Nape, R. de Mello Koch, and A. Forbes, "Topological rejection of noise by quantum skyrmions," Nat. Commun. **16**(1), 2934 (2025).

[43]We use a hat to denote the density matrix in order to distinguish it from the radius in polar coordinates.

[44]Specifically, our analysis assumes an entangled wave function of two systems, A and B, of the form $|f_1(r_A)\rangle|H\rangle_B + \exp(i\alpha)|f_2(r_A)\rangle|V\rangle_B$, for any f_1 and f_2.

[45]We do not consider fluctuations of the relative phase, but these can easily be included. Our motivation for ignoring this possibility is simply the fact that the skyrmion number is completely insensitive to α.

[46]M. A. Nielsen and I. L. Chuang, *Quantum Computation and Quantum Information* (Cambridge University Press, Cambridge, 2001), Vol. 2.

[47]K. Kraus, A. Böhm, J. D. Dollard, and W. Wootters, *States, Effects, and Operations Fundamental Notions of Quantum Theory*, *Lectures in Mathematical Physics at the University of Texas at Austin* (Springer, 1983).

[48]H.-P. Breuer and F. Petruccione, *The Theory of Open Quantum Systems* (Oxford University Press, Oxford, 2002).

[49]A. Rivas and S. F. Huelga, *Open Quantum Systems* (Springer, 2012), Vol. 10.

[50]A. Z. Goldberg, "Quantum theory of polarimetry: From quantum operations to Mueller matrices," Phys. Rev. Res. **2**(2), 023038 (2020).

[51]In what follows, a hat is used to denote an operator.

[52]The group SL(2, $\mathbb{C}$) consists of all 2 × 2 complex matrices with determinant 1. There is a two-to-one homomorphism between SL(2, $\mathbb{C}$) and the proper

19 May 2025 14:12:42

© Author(s) 2025

orthochronous Lorentz group $SO^+(1, 3)$, which is the subgroup of the Lorentz group that preserves the orientation of space and the direction of time. This means that each element of $SO^+(1, 3)$ corresponds to two elements in $SL(2, \mathbb{C})$. Some of the manipulations below have a transparent interpretation, bearing this connection in mind.

[53] This connection simply reflects the fact that the Stokes parameters are in the 4-vector $(\frac{1}{2}, \frac{1}{2})$ representation of the Lorentz group. Indeed, the indices of the Pauli matrices are in the $(\frac{1}{2}, 0)$ and the $(0, \frac{1}{2})$ and $(\frac{1}{2}, 0) \otimes (0, \frac{1}{2}) = (\frac{1}{2}, \frac{1}{2})$.

[54] It is often stated that many Jones matrices correspond to one Mueller matrix because R_{ij} is independent of the overall phase of J. This independence of the phase is already present at the level of the density matrix, and we never distinguish states that only differ by an overall phase. Therefore, at the quantum level, the phase of the Jones matrix (which for us is a Kraus operator) is not physical.

[55] Familiar group theory of $SO^+(1, 3)$ is again apparent. The rotation R_{ik} rotates the spatial components of the 4-vector in $(\frac{1}{2}, \frac{1}{2})$, while the Jones matrix is the same transformation in the $(\frac{1}{2}, 0)$ representation.

[56] O. Gamel and D. F. V. James, "Causality and the complete positivity of classical polarization maps," Opt. Lett. **36**(15), 2821–2823 (2011).

[57] B. N. Simon, S. Simon, F. Gori, M. Santarsiero, R. Borghi, N. Mukunda, and R. Simon, "Nonquantum entanglement resolves a basic issue in polarization optics," Phys. Rev. Lett. **104**(2), 023901 (2010).

[58] S. R. Cloude, "Group theory and polarisation algebra," Optik **75**(1), 26–36 (1986); available at http://pascal-francis.inist.fr/vibad/index.php?action=getRecordDetail&idt=8138457.

[59] We thank the anonymous referee for this example.

[60] B. C. Hall, *Lie Groups, Lie Algebras, and Representations, An Elementary Introduction* (Springer, New York, 2015).

[61] We thank the anonymous referee for their insightful comments on this point.

[62] The points at infinity have $\rho = \infty$ and any ϕ value.

[63] B. Ndagano, I. Nape, M. A. Cox, C. Rosales-Guzman, and A. Forbes, "Creation and detection of vector vortex modes for classical and quantum communication," J. Lightwave Technol. **36**(2), 292–301 (2018).

[64] C. Rosales-Guzmán, B. Ndagano, and A. Forbes, "A review of complex vector light fields and their applications," J. Opt. **20**(12), 123001 (2018).

[65] H.-J. Wu, B.-S. Yu, Z.-H. Zhu, C. Rosales-Guzmán, Z.-Y. Zhou, D.-S. Ding, W. Gao, and B.-S. Shi, "Heralded generation of vectorially structured photons with a high purity," Front. Phys. **9**, 654451 (2021).

[66] K. Y. Bliokh, F. J. Rodríguez-Fortuño, F. Nori, and A. V. Zayats, "Spin–orbit interactions of light," Nat. Photonics **9**(12), 796–808 (2015).

[67] A. McWilliam, C. M. Cisowski, Z. Ye, F. C. Speirits, J. B. Götte, S. M. Barnett, and S. Franke-Arnold, "Topological approach of characterizing optical skyrmions and multi-skyrmions," Laser Photonics Rev. **17**(9), 2300155 (2023).

19 May 2025 14:12:42

© Author(s) 2025